

**DEVELOPMENT OF CAR PISTON MATERIAL FROM ALUMINIUM ALLOY  
USING COCONUT SHELL ASH AS AN ADDITIVE**

**BY**

**ABBA-AJI, Mala Ali  
PhD/SEET/2016/874**

**A THESIS SUBMITTED TO THE POSTGRADUATE SCHOOL  
FEDERAL UNIVERSITY OF TECHNOLOGY, MINNA, NIGERIA IN PARTIAL  
FULFILLMENT OF THE REQUIREMENTS FOR THE AWARD OF THE  
DEGREE OF DOCTOR OF PHILOSOPHY (PhD) IN INDUSTRIAL AND  
PRODUCTION ENGINEERING**

**AUGUST, 2021**

## ABSTRACT

This research presents the development of a piston material from aluminium alloy using coconut shell ash as an additive. Most damage pistons reported in literature are as a result mechanical fatigue due to wear and thermal fatigue. Investigations revealed that aluminium alloys have relatively poor wear resistance, and researchers are concerned with reinforcing aluminium alloy for improved properties. The present work used coconut shell ash for the reinforcement. The coconut powder was produced by crushing the coconut shell which was sieved to a particle sizes (below 70 micron) for the composite. The powder was then subjected to firing in an oven to obtain the ash. Aluminium alloy (Al 356-T7) was used as the matrix, while the coconut shell ash was the reinforcing material. The composites were prepared using double-stir casting method. The aluminium alloy was heated to about 750<sup>0</sup>C and the coconut shell ash, which was preheated to about 800<sup>0</sup>C was added in the proportion of 3, 6, 9, 12 and 15W% to produce the composites. The composites were machined into standard sizes for the purpose of determining the mechanical properties; tensile strength, hardness wear rate and thermal behaviour. The results obtained show that addition of the coconut shell ash particles reinforcement to the alloy increased the tensile and hardness value of the composite but reduced its wear rate and density. The coconut shell ash reinforced piston was produced and was tested using 12-valve model E series automobile engine in terms of performance and failure rate. The results obtained show a fuel consumption savings of 0.036 litre per minute, which is similar to that of conventional piston. The composite can find application in automotive components like brake system where lightweight materials are required with good wear resistance, strength and hardness.

## TABLE OF CONTENT

Content	
Page	
Title page	i
Declaration	ii
Certification	iii
Dedication	iv
Acknowledgements	v
Abstract	vi
Table of Content	vii
List of Tables	xii
List of Figures	xiii
List of Plates	xiv
Symbols	xv
<b>CHAPTER ONE</b>	
<b>1.0 INTRODUCTION</b>	<b>1</b>
1.1 Background to the Study	2
1.2 Statement of the Problem	2
1.3 Aim and Objectives	3
1.4 Justification of the Study	3
1.5 Scope of the Study	4
<b>CHAPTER TWO</b>	
<b>2.0 LITERATURE REVIEW</b>	<b>5</b>
2.1 Metal Matrix Composites (MMCs)	5

2.1.1 Mechanical Properties of MMCs	7
2.1.2 Properties of Aluminium Matrix Composites (AMCs)	8
2.1.3 Effect of Ceramic Reinforcement on the behaviour of AMCs	10
2.1.4 Intrinsic Effects of Ceramic Reinforcements	10
2.1.5 Extrinsic Effects of Ceramic Reinforcement	11
2.1.6 Applications of AMCs	11
2.1.7 Wear behaviour of aluminium-based metal matrix composites	13
2.2 Car Engine Piston	13
2.2.1 Piston Crown	15
2.3.0 Types of Aluminium Matrix Composites	21
2.3.1 Particle reinforced Aluminium Matrix Composites (PAMCs)	21
2.3.2 Short Fibre and Whisker-Reinforced Aluminium Matrix Composites (SFAMCs)	22
2.3.3 Continuous Fibre-Reinforced Aluminium Matrix Composites	23
2.3.4 Monofilament Reinforced Aluminium Matrix Composites	23
2.4 Fly Ash Classification	23
2.4.1 Coal Rank	24
2.4.2 The SiO <sub>2</sub> -Al <sub>2</sub> O <sub>3</sub> -CaO (SAC) Ternary	25
2.5.0 Review of Related Past Work	28
2.6 Research Gap	42
<b>CHAPTER THREE</b>	
<b>3.0 MATERIALS AND METHODS</b>	
3.1. Materials and Equipment	43
3.1.1 Materials	43
3.1.2 Equipment and Tools	43

3.2.0 Methods	44
3.2.1 Processing of Coconut shell ash	44
3.2.2 Particle Size Analysis	45
3.2.3 Thermal Analysis	45
3.2.4 Density Measurement	46
3.2.5 Hardness Test	46
3.2.6 Tensile and Wear Test	47
3.2.7 Wear Test:	47
3.2.8 Determination of Coefficient of Friction	48
3.2.9 Corrosion Test	48
3.3 Design Analysis and Calculation of Piston Parameters	50
3.3.1 Determination of Thickness of the Sealing Part of the Piston	50
3.3.2 Estimation of the Piston Crown Radius	50
3.3.3 Determination of Stress Acting on the Piston Crown	51
3.3.5 Determination of Linear Velocity of the Piston	52
3.3.6 Determination of the piston head thickness	52
3.3.7 Analysis of Piston Rings	53
3.3.8 Determination of the Minimum Axial Thickness of the Piston Rings	54
3.3.9 Analysis of the Piston Barrel (skirt)	54
3.3.10 Determination of length of piston pin in the connecting rod bushing	55
3.3.11 Determination of piston pin diameter	55
3.4 Composite Preparation using Stir Casting	56

3.5.0 Piston Machining Process	57
3.5.1 Pinhole Boring	58
3.5.2 Turning	58
3.5.3 Drilling and Grinding	58
3.5.4 Deburring and Tin Coating	59
3.5.5 Reaming	59
3.6 Calculating RPM for Reaming	60
3.7.0 Performance Test on the Piston	61
3.7.1 Idle and low speed engine performance test experiment, using MMC piston	61
<b>CHAPTER FOUR</b>	
<b>4.0 RESULTS AND DISCUSSION</b>	63
4.1 Particle Size Analysis Results	63
4.2 Microstructural Analysis of Composites	64
4.3 Thermal Behaviour	70
4.4 FTIR analysis of the coconut shell ash particles	72
4.5 Composite Hardness Values	73
4.6 Tensile and Yield Strength Test Values	74
4.7 Density Values of the Composites	74
4.8 Wear behaviour and Coefficient of Friction	77
4.9 Corrosion Behaviour	82
4.10 Performance Test	83
4.11 Validation of Result	88
<b>CHAPTER FIVE</b>	

<b>5.0 CONCLUSIONS AND RECOMMENDATIONS</b>	91
5.1 Conclusion	91
5.2 Recommendations	93
References	94
Appendices	100
A1: Variation of Hardness values with wt% Coconut Shell Ash Particles	100
A2: Variation of Tensile strength with w% coconut shell ash particle	100
A3: Density with percent increment of Coconut Shell Ash	101
A4: Variation of wear rate with wt% of coconut shell ash particles	101
A5: Variation of Coefficient of Friction with w% of Coconut Shell Ash	102
A6: Average Corrosion Rate Al-Si-Fe/Coconut Shell Ash (CSAp) Composites Immersed In 3.5% NaCl Solution	102
B1: Fuel Consumption per KWh for Conventional Standard Piston 103	
B2: Fuel Consumption per KWh of the Produced Composite Piston	103

## LIST OF TABLES

Tables	Pages
2.1: Causes of Piston Damages	16
2.2: Chemical Requirement	26
2.3: Properties of Aluminium 356-T7	27
2.4: Chemical Composition of Aluminium Alloy	27
2.5: Meta-Analysis of Selected Literature	39
3.1: Engine Specifications	50
4.1: Composition of Coconut Shell Ash	64
4.2: Hardness Test Results of the Composites	74
4.3: Tensile and Yield Strength at 0.2% Upset	74
4.4: Density of the Composites	77
4.5: Wear Rate of the Composites ( $\text{mm}^3/\text{Nm}$ )	79
4.6: Coefficient of Friction of the Composites at Different Loads and Wt%CSAp	80
4.7: Average Values for Weight Loss (mg) of the Composite Immersed in 3.5% by Weight NaCl Solution	82
4.8: Performance Test (Standard Piston)	84
4.9: Performance Test (Mmc Piston)	85
4.10: Properties of Produced MMC Piston with Previous Research	88
4.11: Hardness Test Comparison	90



## LIST OF FIGURES

Figures	Page
2.1: Classification of Metal Matrix Composites	6
2.2: Schematic diagram for sliding wear ball on disc tests.	13
2.3: Section of a Piston	14
2.5: SAC Ternary Diagram	24
3.1: Sketch for the Corrosion Test Apparatus.	49
3.2: Flow Chart for Piston Machining	57
4.1: EDS of CSA Particles	63
4.2: EDS of Aluminium Alloy	64
4.3: EDS of 3% by weight CSAP	65
4.4: DTA/TGA of Al-Si-Fe Alloy	70
4.5: DTA/TGA of Al-Si-Fe Alloy/15% by Weight CSAP	71
4.6: FTIR Spectrum of the Coconut Shell Ash	73
4.7: Performance Evaluation of Conventional and MMC Piston	86
4.8: Variation of Brake force with Engine speed ratio	87
4.9: Comparison of Properties of Produced MMC Piston with Previous Research	89

## LIST OF PLATES

Plates	Pages
I     Some Industrial Applications of AMCs	12
II    The Three Common Shapes of Piston Head	16
III   (a) Crushed (b) Ground Coconut Shell	44
IV    (a) Coconut Shell Powder (b) Coconut Shell Ash	45
V     Cast Composite Piston	57
VI    Photograph Toyota Model 12 valve engine	61
VII   SEM Spectrum of Coconut Shell Ash	63
VIII  SEM of the Aluminium Alloy	64
IX    SEM/EDS of the Aluminium Alloy with 3% by Weight CSAp	65
X     SEM of the Aluminium Alloy with 6% by Weight CSAp	65
XI    SEM of the Aluminium Alloy with 9% by Weight CSAp	66
XII   SEM of the Aluminium Alloy with 12% by Weight CSAp	66
XIII  SEM of the Aluminium Alloy with 15% by Weight CSAp	67
XIV   SEM Fractographs of the Aluminium Alloy	75
XV    SEM Fractographs of the Aluminium Alloy Reinforced with 15wt% CSAp	76
XVI   SEM of the Worn Surface of the Aluminium Alloy at 50N, 2.0m/s and 4000m.	77
XVII  SEM of the Worn Surface of the Aluminium Alloy with 9% by Weight CSAp at 50N, 2.0m/s and 4000m of Varied Applied Load	78

## SYMBOLS

Symbols	Definitions	Symbols	Definitions
D	Piston Bore diameter	$p_{pr}$	Maximum Pressure
$\updownarrow$	Piston Stroke	$\sigma_t$	Permissible Tensile Stress
X	Displacement	L	Length of Piston
CR	Compression ratio	FOS	Factor of Safety
P	Maximum Power	b	Radial Width
T	Maximum Torque	CS	Cutting Speed
n	Number of Revolution per Cycle	$D_z$	Diameter of Cutter
S	Thickness of Sealing Part	$V_f$	Table Feed
$r_i$	Crown Inner Radius	$f_z$	Recommended Feed
dt	Radial Clearance	z	Number of Cutting Tool Teeth
$t_R$	Radial Thickness	$\delta$	Thickness of the Piston Crown
$\sigma_b$	Stress acting on Piston Crown	N	Perpendicular Force
Mb	Maximum Bending Moment	$F_r$	Resistive Force
Pmax	Maximum Pressure	$\mu$	Coefficient of Friction
WR	Wear Rate		
$\omega$	Angular Velocity		
rpm	Revolution per Minute		
t	Time		
$t_H$	Piston Head Thickness		

## CHAPTER ONE

### 1.0

### INTRODUCTION

#### 1.1 Background to the Study

A piston is a moving component that is contained by a cylinder and is made gas tight by piston rings. In an engine its purpose is to transfer energy from expanding gas in the cylinder to the crankshaft via piston rod or connecting rod. Pistons are composed of a special aluminium alloy and some other metal elements. They change into sophisticated products after going through different phases and meeting international standards. Manufacturers are required to produce pistons with reduced air pollution, lower density and higher efficiency for fuel and oil; consequently such pistons should have high solidity and low weight. The engine can be called the heart of a vehicle and the piston may be considered the most important part of an engine. As an important part in the engine, piston endures the cyclic gas pressure and inertia forces at work. This working condition may cause the fatigue damage of the piston. Investigations indicate that greatest stress appears on the upper part of the piston and stress concentrations is one of the main reasons for fatigue failure (Venkata, *et al.*, 2013).

Coconut (*Cocos nucifera*) can be obtained from oil palm tree found to thrive well in the tropical rainforest of Nigeria, and has been used as a composites material by Chinthani and Mevan, (2015), and Poornesh *et al.* (2017). Composites have been defined as a multiphase material that exhibits a significant property of constituent phases such that a better combination of properties can be realized (Callister, 2013).

The property of composite materials is thought to be a combination of the properties of both constituent phases, although this is not always the case with respect to certain

properties such as toughness. The overall result will yield an entirely different material with the combination of properties such as lightweight, high strength, stiffness, good corrosion and abrasion resistance. These properties are rare combination compared to those found in the conventional iron and steel used in virtually every aspect of modern human life. The advent of composite materials has brought relief to the automobile industries and indeed the entire world by the use of lightweight materials with comparatively high strengths to heavy steels. Moreover, hybrid technologies that combine electricity with internal combustion engines such as lightweight vehicle will produce enormous oil saving thereby reducing hazardous emission such as carbon monoxide into the atmosphere and increasing efficiency as well. The study of composites is a dynamic one because research activities can continually be carried out by regulation of composite manufacturing parameters and constituents until the optimum characteristics have been attained. For example, the input of additives and fillers such as chemicals and minerals in various proportions show some improvement in the physical and mechanical properties of composites, (Enetanya, 2014).

## **1.2 Statement of the Problem**

There are lots of research work on engine pistons, new geometries, materials and manufacturing techniques, and this evolution has undergone with a continuous improvement over the last decades, and required thorough examination of the smallest details. Notwithstanding all these studies, there are a huge number of damaged pistons. Damage mechanisms have different origins and are mainly wear, temperature and fatigue related. The fatigue related piston damages play a dominant role mainly due to thermal and mechanical fatigue either at room or at high temperature. The present research intends to improve the strength, density and temperature resistance, by introducing a

locally sourced material, coconut shell, as reinforcement to aluminium alloy in the piston production.

The availability of coconut shell is increasing every year worldwide, which is a hard lignocellulose Agro waste. Nigeria is one of the largest producers of coconut. But mostly the coconut shells are left out in the garbage or burnt as waste and produce large quantity of CO<sub>2</sub> and methane emission (Udhayasankar and Karthikeyan, 2015).

### **1.3 Aim and Objectives of the Study**

The aim of this research is to develop a car engine piston material from aluminium alloy using coconut shell as additive. The objectives are to:

- i. Produce an aluminium alloy with coconut shell ash composite for car piston production
- ii. Develop a piston using aluminium alloy and coconut shell ash composite produced
- iii. Investigate the mechanical properties and thermal behaviour of the existing piston and compare with the Aluminium Matrix Composite (AMCs) of the coconut shell ash
- iv. Carry out the performance evaluation of the produced piston from the coconut shell aluminium matrix composite (AMC) in terms of failure and fuel economy and compare it to that of the existing piston.

### **1.4 Justification of the Study**

Metal matrix composites (MMCs) maintained a significantly improved properties, comprising high specific strength, specific modulus, damping capacity and good wear resistance, when compared to unreinforced alloys. Similarly, there has been an increasing interest in composites containing low density and low cost of reinforcements.

The present research is geared towards utilizing coconut shell ash as composite for aluminium alloys, for piston production. The use of coconut shell reinforced materials offer several environmental advantages, such as decreased dependence on non-renewable material sources, lower pollution and green house emission. The advantages of coconut shell ash over conventional reinforcing materials (glass and carbon) are low cost and low density. (Chinthani and Mevan, 2015)

### **1.5 Scope of the Study**

The present study is limited to the development of a reinforced aluminium composite using coconut shell ash as additive for car piston production. The tests to be carried out to investigate the properties of the produced metal matrix composite (MMC) are limited to tensile and yield strength, hardness, density, corrosion, wear resistance and thermal behaviour.

## CHAPTER TWO

### 2.0 LITERATURE REVIEW

#### 2.1 Metal Matrix Composite (MMC)

A great deal of research work has been carried out on composite materials at various levels and places. Aluminium based alloys are widely used in applications where weight savings are important. However, the relatively poor wear resistant of aluminium alloys has limited their use in certain high friction environments (Kenneth *et al.*, 2018).

Literature available on the subject revealed that most of the studies have been carried out to evaluate the wear behaviour of aluminium based particulate or whisker reinforced composites. It is generally agreed that various applications of aluminium matrix composites (AMCs) such as aerospace (satellite struts), defence (electronic instrument racks), automobile (drive shafts and brake discs), sport goods (golf clubs and mountain bicycle frames), and marine (yacht fittings) are created by reinforcement and also wear properties are improved remarkably by introducing hard intermetallic compound into the aluminium matrix. The reinforcing materials are generally silicon carbide SiC, aluminium oxide Al<sub>2</sub>O<sub>3</sub>, titanium boride TiB<sub>2</sub> and graphite (Oghenevweta *et al.*, 2016).

The use of graphite reinforcement in a metal matrix has the potential to create a material with high thermal conductivity, excellent mechanical properties and attractive damping behaviour at elevated temperatures. However, lack of wettability between aluminium and the reinforcement, and oxidation of the graphite, lead to manufacturing difficulties and cavitation of the material at high temperature (Pardeep *et al.*, 2016).

Alumina (Clyne, 2013) and other oxide particles like Lithium Oxide (LiO<sub>2</sub>) have been used as reinforcing particles in Al-matrix. Alumina has received attention as a reinforcing



phase as it is found to increase the hardness, tensile strength and wear resistance of aluminium metal matrix composites. Oghenevweta *et al.* (2016), Clyne (2013) and Pardeep *et al.* (2016) studied mica, alumina, and silicon carbide, clay, zircon, and graphite as reinforcements in the production of composites. Numerous oxides, nitrides, borides and carbides were studied by Vorozhtsov *et al.* (2015), as reinforcements for high temperature discontinuously reinforced aluminium (HTDRA). It has been inferred from their studies that HTDRA containing TiC, TiB<sub>2</sub>, B<sub>4</sub>C, SiC and Si<sub>3</sub>N<sub>4</sub> exhibit the highest values of specific stiffness.

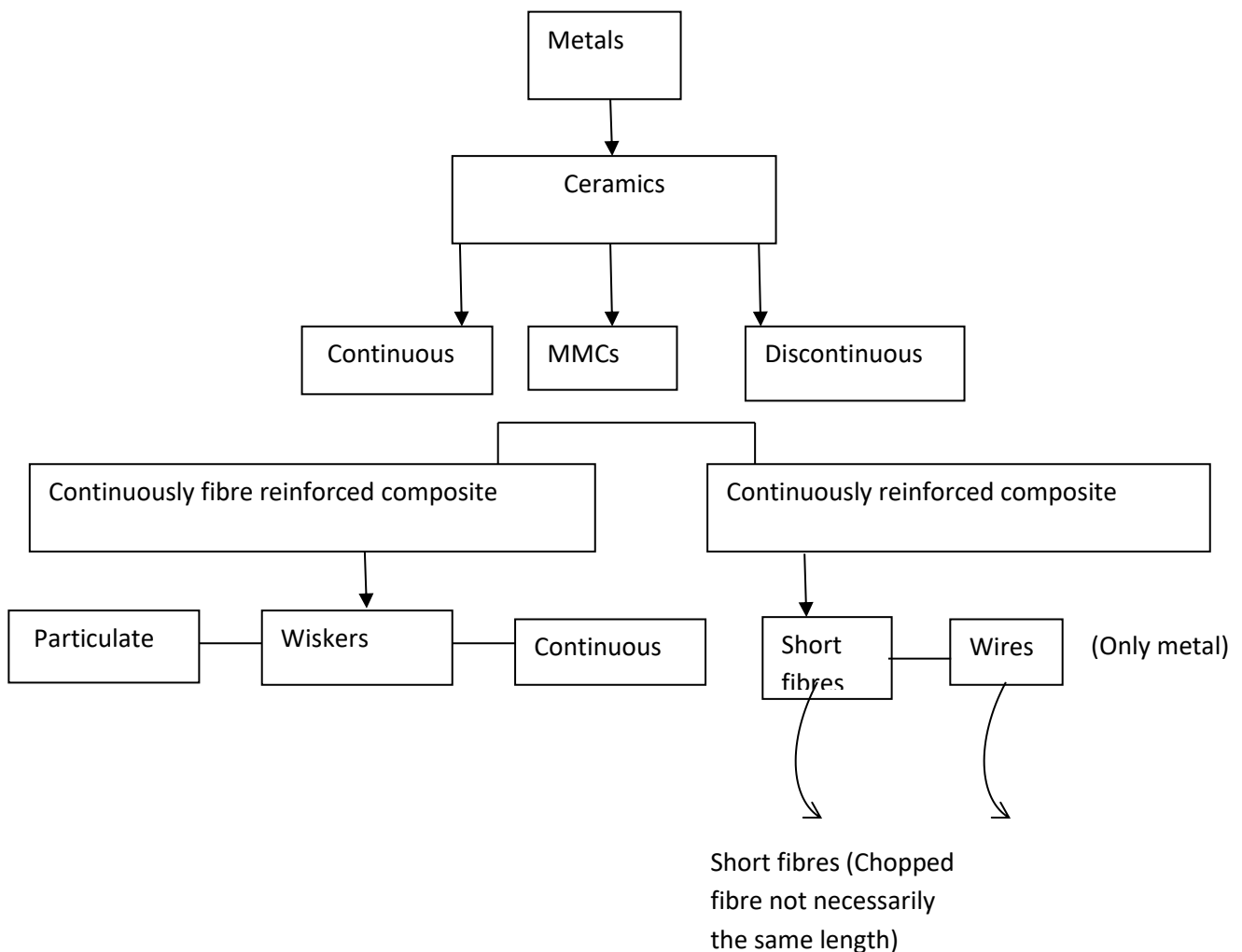


**Fig. 2.1: Classification of Metal Matrix Composites (Clyne, 2013)**

It has been proven that ceramic particles are effective reinforcement materials in aluminium alloy to enhance mechanical and other properties. The reinforcement in MMCs is usually of ceramic materials; these reinforcements can be divided into two major groups, continuous and discontinuous (Figure 2.1). The MMCs produced by the reinforcements are called continuously (fibre) reinforced composites and discontinuously reinforced composites (Clyne, 2013). However, they can be subdivided broadly into four major categories.

- i. Continuous fibres,
- ii. short fibres (chopped fibres, not necessarily of the same length),
- iii. whiskers,
- iv. Particulate and wire (only for metal) Figure 2.1.

With the exception of wires, reinforcements are generally ceramics, typically these ceramics being oxides, carbides and nitrides. They are used because of their combinations of high strength and stiffness at both room and elevated temperatures. Common reinforcement elements are Silicon (SiC), Aluminium Oxide ( $Al_2O_3$ ), Titanium Bromide ( $TiB_2$ ), boron and graphite will persist because many of the aspects cited above in addition to contamination from processing equipment and feedstock may vary greatly (Clyne, 2013). Since most ceramics are available as particles, there is a wide range of potential reinforcements for particle reinforced composites.

### **2.1.1 Mechanical Properties of MMCs**

Metal matrix composites (MMCs) have emerged as a class of materials for advanced structural, aerospace, automotive, electronic, thermal management and wear applications. The performance advantage of metal matrix composites is tailored to their mechanical, physical and thermal properties that include low density, high specific strength, high

specific modulus, high thermal conductivity, and high abrasion and wear resistance. In general, the reduced weight and improved stiffness of the MMCs are achieved with various monolithic matrix materials. The attractive physical and mechanical properties that can be obtained with metal matrix composites, such as high specific modulus, strength and thermal stability, have been documented extensively (Oghenevweta *et al.*, 2016). The various factors controlling the properties of particulate MMCs and the influence of the manufacturing methods on the MMCs properties have also been reviewed by several investigators. Improvement on modulus, strength, fatigue, creep, thermal and wear resistance properties have already been demonstrated for a variety of reinforcements (Oghenevweta *et al.*, 2016). Among these properties, tensile strength is most convenient and widely quoted, and is of central importance in many applications.

The strength of particle-reinforced composites is observed to be most strongly dependent on the volume fraction and particle size of the reinforcement. Dislocation strengthening will play a more significant role in the MMCs than in the reinforced alloy due to the increased dislocation density. The high temperature creep strength of materials is also greatly improved by the addition of a high temperature stable disperse phase, due to grain boundary pinning. Grain refinement is not desirable in high temperature materials as it results in a higher rate of grain boundary sliding, which is an important mechanism of creep. For this reason, dispersion strengthening is of particular importance in creep resistant metals such as oxide dispersion strengthened super alloy (Vorozhtsov *et al.*, 2015).

### **2.1.2 Properties of Aluminium Matrix Composites (AMCs)**

The major advantages of AMCs compared to unreinforced aluminium alloy are as follows; greater strength, improved stiffness, reduced density (weight), controlled thermal

expansion coefficient, thermal/heat management, enhanced and tailored electrical performance (Clyne, 2013).

AMCs have improved abrasion and wear resistance, control of mass (especially in reciprocating application), and improved damping capabilities.

These advantages are quantified for better appreciation. For example, elastic modulus of pure aluminium can be enhanced from 70GPa to 240GPa by reinforcement with 60% by volume. Continuous alumina fibre in pure aluminium, leads to decrease in the coefficient of expansion (Fernando and Hans, 2010). Similarly, it is possible to process Al-9% by volume Si-20% by volume SiC particulate composites having wear resistance equivalent or better than that of grey cast iron (Clyne, 2013). All these examples illustrate that it is possible to alter several technological properties of aluminium/aluminium alloy by more than two to three orders of magnitude by incorporating appropriate reinforcement in suitable volume fraction. AMC material systems offer superior combinations of properties in such a manner that today no existing monolithic material can rival them.

Over the years, AMCs have been tried and used in numerous structural, non-structural and functional applications in different engineering sectors (Razzak *et al.*, 2017). The driving force for the utilization of AMCs in these sectors includes performance, economic and environmental benefits. The key benefits of AMCs in the transportation sector are lower fuel consumption, less noise and lower airborne emissions. With increasing stringent environmental regulations and emphasis on improved fuel economy, use of AMCs in the transport sector will be inevitable.

AMCs are intended to substitute monolithic materials including aluminium alloys, ferrous alloys, titanium alloys and polymer based composites in several applications. In order that AMC substitution for monolithic materials in engineering systems is

widespread, there is a compelling need to redesign the whole system to gain additional weight and volume savings. In fact, according to the United Kingdom (UK) Advisory Council on Science and Technology and American Society for Testing and Materials (ASTM D 388), AMCs can be viewed either as replacements for existing materials, but with superior properties, or as a means of enabling radical changes in system or product design. Moreover, by utilizing near-net shape forming and selective-reinforcement techniques. AMCs can offer economically viable solutions for a wide variety of commercial applications. Recent successes in commercial and military applications of AMCs are based partly on such innovative changes made in component design. Lack of adequate information and research have hindered the public from the utilization of service properties and possible usage of (AMCs) (Fernando and Hans, 2010).

### **2.1.3 Effect of ceramic reinforcements on the behaviour of aluminium matrix in AMCS**

The presence of a relatively large (more than 10%) volume fraction of ceramic reinforcement (whisker, particle, short fibre and continuous fibre) profoundly affects the behaviour of aluminium matrix in aluminium matrix composites during manufacturing, heat treatment and their subsequent use in service. These changes include both intrinsic and extrinsic ones (Fernando and Hans, 2010).

### **2.1.4 Intrinsic Effects of Ceramic Reinforcements**

Intrinsic effects include microstructural changes, heat treatment characteristics and thermal stresses. These changes significantly alter and expand the physical, mechanical and tri-biological property limits of aluminium alloy (Clyne, 2013).

The presence of ceramic reinforcement can alter the solidification behaviour of aluminium alloys in several ways. Ceramic reinforcement can serve as a barrier to

diffusion of heat and solute, catalyse the heterogeneous nucleation of phases crystallizing from the melt, restrict fluid convection and induce morphological instabilities in the solid-liquid interface.

Aluminium matrix composites often experience fabrication temperature in excess of 500<sup>0</sup>C, and large thermal residual stresses are included on cooling. The magnitude of thermal residual stresses developed is related to many variables including the type of reinforcement, volume fraction, diameter and aspect ratio. For example, thermal residual stresses (tensile) of more than 100 MPa are present in the matrix of Al-30% by volume SiC particulate composites. Mechanical behaviour of AMCs is profoundly affected by thermal residual stresses. The presence of residual stresses caused by ceramic reinforcements results in a symmetrical yielding, and also affect fatigue and creep behaviour (Fernando and Hans, 2010).

#### **2.1.5 Extrinsic effects of ceramic reinforcement**

Incorporation of ceramic reinforcement in aluminium alloys leads to significant improvement in the sliding wear resistance of AMCs as measured by the pin-on-disc set up against a hardened steel disc (Clyne, 2013).

In recent years the extrinsic effect of SiC reinforcement in AMCs has been beneficially utilized in brake disc/brake pad tribo couples. When the AMCs brake disc slides against the brake pad adherent tribo layers are formed on the surface of the AMCs disc at the contact region. Tribo layers thus formed, further enhance the wear resistance of the AMC discs. Tribo layers consisting of mixed oxides are formed due to the transfer of material from the brake pad on to the AMCs disc during sliding (Clyne, 2013).

### 2.1.6 Applications of AMCs

AMCs now have a proven track record as successful "high-tech" materials in a range of applications. AMCs utilization provides significant benefits including performance benefits (component lifetime, improved productivity), economic benefits (energy savings or lower maintenance cost) and environmental benefits (lower noise levels and fewer air-borne emissions). Engineering viability of AMCs in a number of applications has been well documented. AMCs having different types of reinforcements (whiskers, particles, short fibres and continuous fibres) have been produced both by solid state and liquid state processing (Francis *et al.*, 2012). The various and numerous applications are mentioned and shown in Plate I (a, b, c &d).

Brake rotors for German high-speed trains ICE-1 and ICE-2 were developed by Knorr Bremse AG and made from a particulate reinforced aluminium alloy (AlSi7Mg+SiC particulates) supplied by Duralcan. Compared to conventional parts made out of cast iron weigh 120 kg per piece: the 76kg of the AMC rotor offers an attractive weight saving potential. The braking systems (discs, drums, calipers or back-plate) of the New Lupo from Volkswagen were made from particulate reinforced aluminium alloy supplied by Duralcan.

AMCs continuous fibre reinforced pushrods were produced by Duralcan for racing engines. These pushrods weigh 40% as much as steel ones; they are stronger and stiffer and have high vibration damping, AMC wires were also developed by Duralcan for the core of electrical conductors. The unique properties of this type of conductor offer substantial performance benefits when compared to the currently used steel wire reinforced conductors.

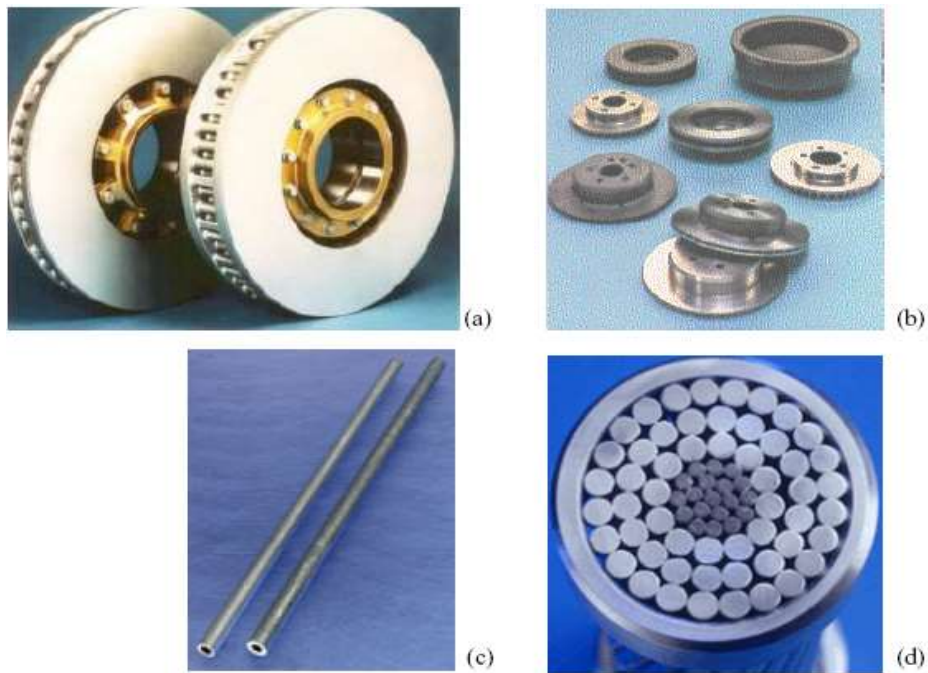


**Plate I:** Some Industrial Applications of AMCs (a) brake rotors for high speed train (b) Automotive braking systems (c) automotive pushrods (d) cores for HV electrical wires. (Francis *et al.*, 2012).

### 2.1.7 Wear behaviour of aluminium-based metal matrix composites

Now a days, aluminium-based metal matrix composites (Al MMCs) are used in making of piston, connecting rod, contactors, where sliding is an important factor. Excessive wear of the mating components sometimes leads to catastrophic failures, so study of wear properties of Al MMCs has become the need of time. Wear tests are generally conducted on ball/pin wear tester, schematic diagram as represented in Figure 2.2. Wear properties of many MMCs having continuous and discontinuous reinforcements like  $\text{Al}_2\text{O}_3$ ,  $\text{MnO}_2$ , SiC, graphite, mica, glass, graphite and others have been reported (Verma and Khvan, 2019)



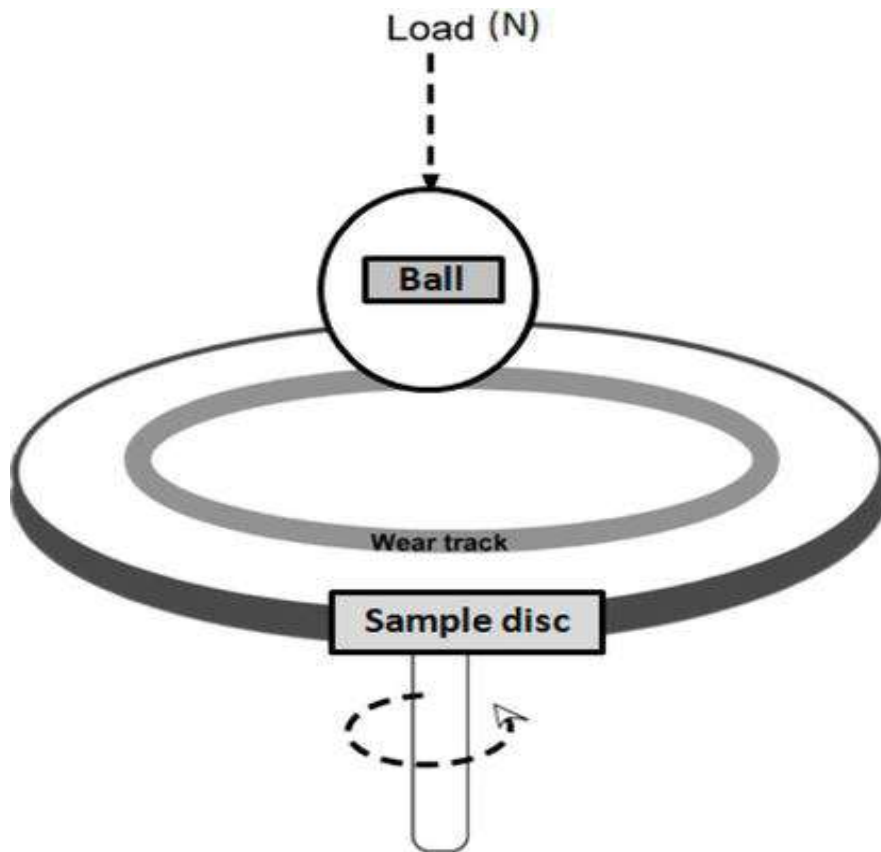
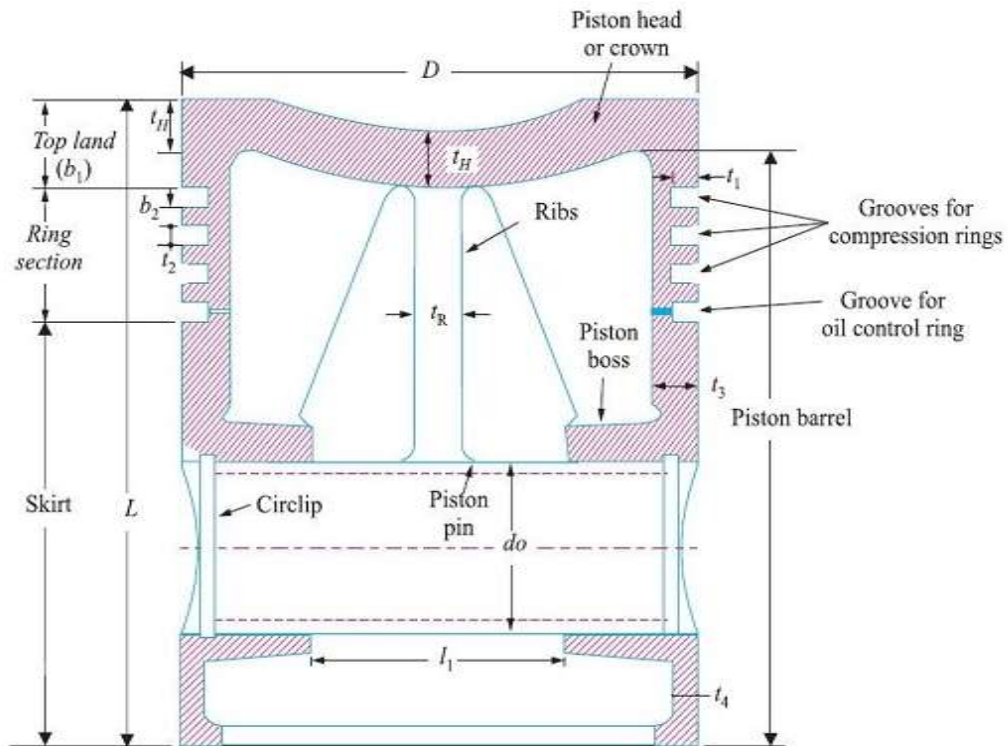


Figure 2.2: Schematic diagram for sliding wear ball on disc tests.

## 2.2. Engine Piston

The piston is a disc which reciprocates within a cylinder. It is either moved by the fluid or it moves the fluid which enters the cylinder. The main function of a piston of an internal combustion engine is to receive the impulse from the expanding gas and to transmit the energy to the crankshaft through the connecting rod. The piston must also disperse a large amount of heat from the combustion chamber to the cylinder walls. The structure of the piston can be divided into two sections, which are the top section and the lower section, Figure 2.1. The top section is known as the head or crown, while the lower section is called the skirt.



**Figure 2.3 Section of a Piston** (Khurmi and Gupta, 2004)

Silva *et al.* (2013) stated that in some engines, the piston also acts as a valve by covering and uncovering ports in the cylinder wall and it can be a carrier for the gas and oil sealing elements (piston rings). The duty cycle, the thermal and mechanical loading, and the requirements of long life and high reliability of the piston assembly represent one of the most arduous sets of conditions for any mechanical component in engineering today. Mechanical and thermal loading are the two types of loading which is applied to pistons during engine operation. Mechanical loading is due to the gas pressure in the cylinder and the reaction from the gudgeoned pin and the cylinder wall.

For thermal loading, it is due to the temperature and heat transfer condition in the cylinder and at other boundaries to the piston. Based on the ignition process in the engine, pistons are subject to high temperatures on one side and relative cold on the other side. It is necessary to understand the loading because this provides the basis for design,

the reason for oil cooling and the cause of structural failure of a piston. In addition to the piston design, material is a major element in the piston manufacturing. The common material that is always used in the manufacturing of piston is aluminium and cast iron. Nowadays, piston is made using aluminium as the raw material compare to cast iron in the early manufacturing of piston. Earlier low speed engine also had pistons of cast iron to match the material used for the cylinder (Silva *et al.*, 2013).

### **2.2.1 Piston Head or Crown**

The crown of the piston is the top surface where the explosive force is exerted when the piston moved up and down in the combustion chamber. Therefore, it is usually thick to resist the high gas pressure and to provide a smooth heat flow from the crown to the combustion rings. The shape of the piston crown depends on the design of the combustion chamber. There are various shapes such as concave, flat, cup, dome, hump and contour to promote turbulence in combustion or to control the combustion process, for example, a piston with an offset of a non-annular bowl is contoured to increase the spray plume length in order to avoid impingement. The shapes of the piston crown are shown in Plate II. Piston damages and their causes are discussed in Table 2.1 (A, B, C & D)



(a)





(b)



(c)

**Plate II: The Three Common Shapes of Piston Head;** (a) Flat Piston Head, (b) Convex Piston Head and (c) Concave Piston Head Respectively (Silva *et al.*, 2013).




**Table 2.1 (A): Causes of Piston Damages** (Kolbenschmidt Motor service Group)

<p><b>Seizure due to overheating (mainly piston crown)</b></p> <p>Overheating due to abnormal combustion</p> <ul style="list-style-type: none"> <li>• Bent/blocked oil splash jet</li> <li>• Installation of incorrect pistons</li> <li>• Faults in the engine cooling system</li> </ul>	 
--	--

**Table 2.1 (B): Causes of Piston Damages** (Kolbenschmidt Motor service)

<ul style="list-style-type: none"> <li>• Restriction of clearances in the upper running surface</li> </ul>	
<p><b>Impact marks</b></p> <ul style="list-style-type: none"> <li>• Excessive piston protrusion</li> <li>• Excessive reworking of the cylinder head mating face</li> <li>• Incorrect valve recess</li> <li>• Incorrect cylinder head gasket</li> <li>• Oil carbon deposits on the piston crown</li> <li>• Insufficient valve clearance</li> </ul>	
<p><b>Material washout in the ring zone</b></p> <ul style="list-style-type: none"> <li>• Incorrectly installed piston rings</li> <li>• Fuel flooding</li> <li>• Severe axial wear of piston ring grooves and piston rings</li> <li>• Piston ring flutter</li> </ul>	

**Table 2.1 (C): Causes of Piston Damages (Kolbenschmidt Motor)**

<p><b>Radial wear due to fuel flooding</b></p> <ul style="list-style-type: none"> <li>• Faults during the mixing stage</li> <li>• Abnormal combustion</li> <li>• Insufficient compression pressure</li> <li>• Incorrect piston protrusion</li> </ul>	
<p><b>Axial wear due to ingress of dirt</b></p> <ul style="list-style-type: none"> <li>• Abrasive dirt particles due to inadequate filtration</li> <li>• Particles of dirt which are not completely removed during an engine overhaul (dwarf, blasting material)</li> <li>• Abraded particles caused when the engine is being run in</li> </ul>	
<p><b>Asymmetric wear pattern of the piston</b></p> <ul style="list-style-type: none"> <li>• Twisted/bent connecting rod</li> <li>• Connecting rod small end bored at an oblique angle</li> <li>• Cylinder bores not straight</li> <li>• Individual cylinders not installed straight</li> <li>• Excessive connecting rod bearing clearance</li> </ul>	

**Table 2.1 (D): Causes of Piston Damages (Kolbenschmidt Motor)**

<p>45° seizure</p> <ul style="list-style-type: none"> <li>• Excessively narrow fit of the piston pin</li> <li>• Seizure in the connecting rod small end (insufficient Lubrication when the engine was first taken into operation)</li> <li>• Incorrectly installed shrink-fit - connecting rod</li> <li>• Excessive load on the engine before it reaches operating Temperature</li> </ul>	
<p><b>Dry-running damage</b></p> <ul style="list-style-type: none"> <li>• Over-rich operation</li> <li>• Abnormal combustion (misfiring)</li> <li>Insufficient compression</li> <li>• Defective cold-starting device</li> <li>• Oil dilution with fuel</li> </ul>	
<p><b>Cavitation</b></p> <ul style="list-style-type: none"> <li>• Poor or inaccurate seating of the liner</li> <li>• Use of incorrect O-rings</li> <li>• Use of unsuitable coolants</li> <li>• Insufficient pre-pressure in the cooling system</li> </ul>	

**Table 2.1 (E): Causes of Piston Damages (Kolbenschmidt Motor)**


<ul style="list-style-type: none"> <li>• Operating temperature too low/too high</li> <li>• Restricted coolantflow</li> </ul>	
<p><b>Shiny marks in the upper part of the cylinder</b></p> <p><b>Oil carbon deposits on the piston top land due to:</b></p> <ul style="list-style-type: none"> <li>• Excessive ingress of engine oil into the combustion chamber due to defective parts</li> <li>• Increased emissions of blow-by gases with oil entering the intake tract</li> <li>• Insufficient separation of oil mist from the blow-by gases</li> <li>• Frequent idle or short journey operation</li> </ul>	

Table 2.1 highlighted some damages encountered by internal combustion engine pistons of high friction. Pistons experience friction with the cylinder walls leading to increase in wear rate. Engine pistons manufacturers use different materials, mostly ceramics and fibre-reinforced materials, to improve the tribological and mechanical properties of piston. The present research used coconut shell ash to reinforce aluminium alloy for engine piston production.



### **2.3.0 Types of Aluminium Matrix Composites**

Aluminium matrix composites (AMCs) can be classified into four types depending on the type of reinforcement (Clyne, 2013)

1. Particle reinforced aluminium matrix composites (PAMCs)
2. Short fibre and whisker reinforced aluminium matrix composites (SFAMCs)
3. Continuous fibre-reinforced aluminium matrix composites (CFAMCs)
4. Monofilament reinforced aluminium matrix composites (MFAMCs)

#### **2.3.1 Particle Reinforced Aluminium Matrix Composites (PAMCs)**

Particle reinforced aluminium metals or particulate reinforced metals are combinations of a metal or alloy with a finite volume fraction of a roughly equiaxed second phase, generally ceramic, that is deliberately introduced into the metal in order to improve its properties. Frequent motivations are to raise the modulus, improve wear resistance, or lower the thermal expansion of aluminium while preserving its low density.

Generally, the improvements that are achieved in the properties of the metal are less extensive than with fibrous reinforcements; however beside the lower cost, these materials present the additional advantages of having generally isotropic properties, and of being compatible with most metal working processes (machining, deformation, processing, welding), particularly when the volume fraction ceramic is below 30 percent. Particle reinforced materials are more attractive due to their cost effectiveness, isotropic properties and their ability to be processed using similar technologies used for monolithic materials (Rao and Raju, 2014).

Particulate reinforcements added to metals are generally ceramic in nature; although in some cases a refractory metal is used (tungsten in copper is an example). The reinforcing particles must, in order to be viable for a given metal, fulfil the following requirements:

(1) They must be comparatively inexpensive. This requirement generally defines both the nature and the form of the particulate reinforcements used in producing engineering PAMCs.

(2) The matrix and reinforcement must not be too mutually reactive (unless an in-situ composite is to be produced): given the intimacy or contact between matrix and reinforcement in the composite, the ceramic must thus be chemically stable in contact with the metal.

(3) Generally, no interfacial reaction is desired, as matrix/particle bonding is in many systems inherently strong without reaction (that is, involves chemical bonds crossing the interface) and is weakened by a finite layer of brittle reaction product(s): hence, systems used are essentially ones of or nil chemical reactivity.

These preconditions generally narrow the list of candidate for reinforcements to only a few possibilities. For the reinforcement of aluminium and its alloys, silica or reinforcements with a significant fraction of silicon (mullite, for example) are not optimal because of (1) their reactivity with the matrix (aluminium and magnesium both reduce silica) and (2) their relatively low elastic modulus compared with that of several alternative ceramics. The two main ceramic particles used as reinforcements for aluminium are: silicon carbide and alumina (Razzak *et al.*, 2017).

### **2.3.2 Short Fibre and Whisker-Reinforced Aluminium Matrix Composites (SFAMCs)**

These contain reinforcements with an aspect ratio of greater than 5, but are not continuous. Short alumina fibre reinforced matrix composite is one of the first and most popular AMCs to be developed and used in pistons. Whisker reinforced composites are produced either by powder metallurgy processing or by the infiltration route.

Mechanical properties of whisker-reinforced composites are superior compared to particle or short fibre reinforced composites. However, in recent years, usage of whiskers as reinforcements in AMCs is fading due to perceived health hazards and hence of late, commercial exploitation of whisker reinforced composites has been very limited. Short fibre reinforced AMCs display characteristics in between those of continuous fibre and particle reinforced AMCs (Clyne, 2013).

### **2.3.3 Continuous Fibre-Reinforced Aluminium Matrix Composites (CFAMCs)**

In continuous fibre reinforcements, the reinforcements are in the form of continuous fibres (of alumina, silicon carbide or carbon). The fibres can either be parallel or pre-woven, braided prior to production of the composite. AMCs having fibre volume fraction up to 40% are produced by the squeeze infiltration technique (Nijssen, 2015)

### **2.3.4 Monofilament Reinforced Aluminium Matrix Composites (MFAMCs)**

Monofilaments are large diameter (100 to 150 $\mu$ m) fibres, usually produced chemical vapour deposition (CVD) of either silicon carbide or carbon into a core of carbon fibre. Bending flexibility of monofilaments is low compared to multifilament. Monofilament reinforced aluminium matrix composites are produced by diffusion bonding techniques and are limited to super plastic, forming aluminium alloy matrices. In continuous fibre-

reinforced aluminium matrix composites and monofilament reinforced aluminium matrix composites, the reinforcement is the principal load bearing constituent, and the role of the aluminium matrix is to bond the reinforcement, transfer and distribute the load (Nijssen, 2015).

## **2.4 Fly Ash Classification**

A key component of North American fly ash classification has long been major element chemistry by weight percentage:  $\text{SiO}_2 + \text{Al}_2\text{O}_3 + \text{Fe}_2\text{O}_3$  in the United State:  $\text{CaO}$  in Canada. The Canadian standards Association (CSA) and the American Society for Testing and Materials (ASTM) recognize two classes of fly ash: Class F, normally produced from high rank coals, and Class C, normally produced from low rank coals. Coal rank has traditionally been an aspect of fly ash classification, particularly the division between low and high rank (John, 2017).

The transition from the current ASTM C 618 specification in the U.S to fly ash classification based on  $\text{CaO}$  (lime), is a necessary and logical step if a more meaningful classification is to be adopted. Iron oxide is essentially a non-reactive component of fly ash and is not expected to be correlated to fly ash performance in concrete. The  $\text{SiO}_2$ - $\text{Al}_2\text{O}_3 - \text{CaO}$  (SAC) ternary diagram accurately predicts fly ash phase mineralogy and is a very useful tool for understanding geochemical variations between fly ashes from differing coal ranks and geological settings. Fly ash measures have been established based on major element chemistry. A simple geochemical variations diagram provides a measure of fly ash alkalinity that correlates relatively closely with the network ratio.

Fly ash classification, based on weight percent  $\text{CaO}$  is a far better approach than the traditional ASTM C 618 standard. The Canadian Standards Association (CSA)

specification of low-intermediate-and high-CaO fly ashes may be a better approach to fly ash classification than the more simplified concept of splitting fly ashes into class F and class C at 18% CaO. (John, 2017)

#### **2.4.1 Coal Rank**

Coal rank as defined by ASTM D 388, is a concept rather than a property and is not measured but is assessed by physical and chemical properties which change during the process of coalification. Rank is the degree of transformation from vegetation to coal. Coalification increases with rank in the sequence peat- lignite – subbituminous – bituminous – semi-anthracite – anthracite – meta-anthracite. High rank coals include bituminous and anthracite. Lignite, also termed “brown coal” and subbituminous coals are the low rank coals

#### **2.4.2 The SiO<sub>2</sub>-Al<sub>2</sub>O<sub>3</sub>-CaO (SAC) Ternary**

As more than 95% of inorganic components of coal consist of the minerals quartz, kaolinite, mullite, calcite, and pyrite. Coal ash is composed primarily of SiO<sub>2</sub>, Al<sub>2</sub>O<sub>3</sub>, CaO, and Fe<sub>2</sub>O<sub>3</sub> with less than 5% of other elements. The SiO<sub>2</sub>-Al<sub>2</sub>O<sub>3</sub>-CaO ternary phase diagram (SAC) as shown in Figure 2.5, is a good predictor of fly ash mineralogy after thermal treatment at 1000<sup>0</sup>C. High rank coal ashes in the mullite field remain largely stable. If 5% to 10% MgO is considered in an additional dimension of the phase diagram, the crystallization of biopsied is expected and observed. At still greater CaO contents, fly ash glass is rapidly crystallized to mullite on heating, as in example of subbituminous coal ashes from the Powder River Basin in America. When MgO is considered, the mullite stability field expands at the expense of feldspar and pyroxene fields.

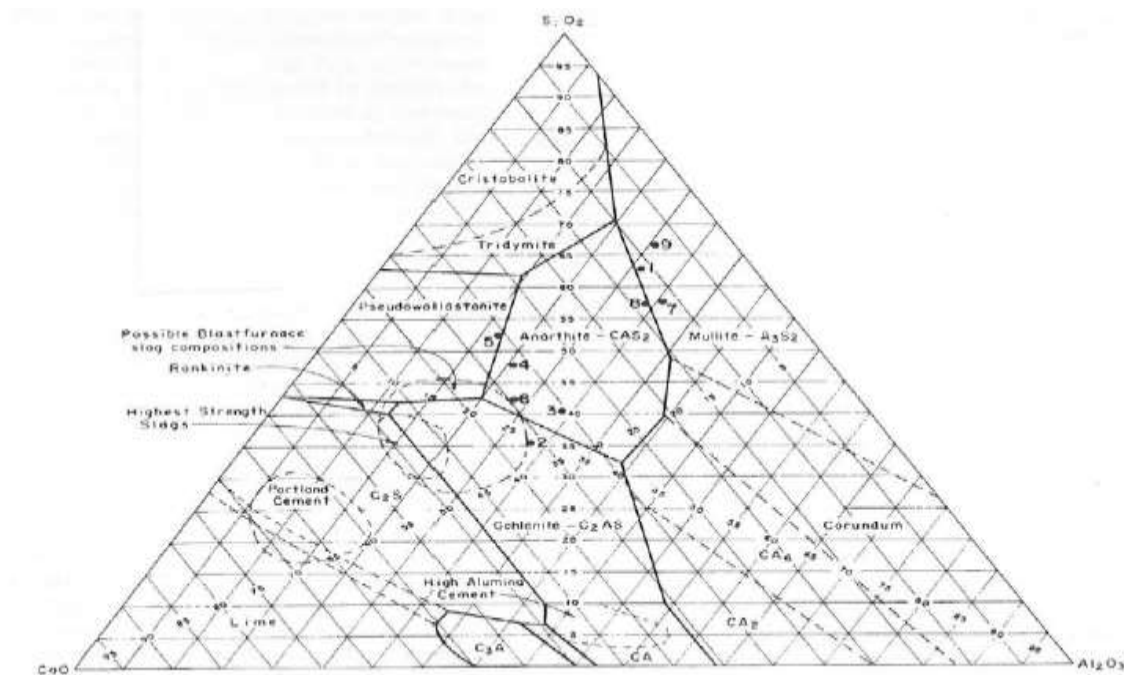


**Figure 2.4: SAC Ternary Diagram (Source: World of Coal Ash (WOCA), Conference, 2017)**

Table 2.2 shows the classification of  $\text{SiO}_2 + \text{Al}_2\text{O}_3 + \text{Fe}_2\text{O}_3$  into C and F according to percentage composition. A percentage composition greater than 50% are classified as C, while percentage composition greater than 70% are classified as F.

**Table 2.2 Chemical Requirement**

S/No.		N	F	C
1	$\text{SiO}_2 + \text{Al}_2\text{O}_3 + \text{Fe}_2\text{O}_3$ , min%	70.0	70.0	50.0
2	Sulphurtrioxide ( $\text{SO}_3$ ), max, %	4.0	5.0	5.0
3	Moisture content, max, %	3.0	3.0	3.0
4	Loss on ignition, max, %	10.0	6.0	6.0

Source: Larry, 2016

•Class C – $\text{SiO}_2 + \text{Al}_2\text{O}_3 + \text{Fe}_2\text{O}_3 \geq 50\%$

•Class F – $\text{SiO}_2 + \text{Al}_2\text{O}_3 + \text{Fe}_2\text{O}_3 \geq 70\%$

•So... Every Class F is a Class C

The difference in ash characteristics at the far extremes of the classification related to calcium oxide (CaO),

1. Class C is cementitious: more  $\text{CaSO}_4$ , free lime,  $\text{C}_3\text{A}$ , calcium, rich glass, MgO

2. Class F (Pozzolanic): more glass, alumina Silicate glass, quartz.

No difference at the margin (Larry, 2016).

Table 2.3 shows the properties of aluminium 356-T7 grade.

**TABLE 2.3: Properties of Aluminium 356-T7**

MATERIAL	ALUMINIUM 356-T7
Thermal Conductivity(W/m-K)	134
Density, (kg/m <sup>3</sup> )	2713
Poisson Ratio	0.35
Coefficient of thermal expansion A (/K)	$18 \times 10^{-6}$
Modulus Of Elasticity (GPa)	72.4
Ultimate Tensile Strength,(MPa)	172

Source: Budynas & Nisbett (2014)

The chemical composition of aluminium alloy is given in Table 2.4.

**Table 2.4 Chemical Composition of Aluminium Alloy**

Material	Al	Cu	Mg	Si	Zn	Fe	Ni
AL Alloy%	Balanced	4-5	0.45-0.65	16-18	1.5	1.3	0.1

Source: American Society for Testing and Materials (ASTM), 2000

## **2.5 Review of Related Past Works**

Prasad and Krishna (2010) worked on the fabrication and characterization of A356.2-rice husk ash (RHA) composite using the stir casting technique. In the study, metal matrix composites (MMC's were prepared by addition of 2, 4, and 8% by weight RHA particulates through the stir casting technique. Mechanical properties like density and hardness for the composites were determined. It was observed that as the percentage of RHA particles increased the density of the composites decreases and there is slight increase in the hardness.

Aigbodion and Hassan (2010) worked on the potential utilization of solid waste bagasse ash. In the study, bagasse ash was chemically and physically characterized in order to evaluate the possibility of its use in industry. Fabricated aluminium composite using a recycled aluminium automotive component and had chosen discarded engine blocks (Al-Si alloy) as a matrix for the composite. The recycled aluminium composite brake disc was found to have significant weight reduction which is about one-third of the conventional cast iron brake disc.

Mahendra *et al.* (2013) conducted a study on evaluation of mechanical properties of aluminium alloy reinforced with silicon carbide and fly ash hybrid metal matrix composites. Increase in area fraction of reinforcement in matrix resulted to improved



tensile strength, yield strength and hardness. Higher percentage of fly ash resulted to decrease of the rate of elongation of the hybrid MMCs.

Gaitondel and Karnik (2012) conducted a study on wear and corrosion properties of Al/Al<sub>2</sub>O<sub>3</sub>/graphite hybrid composite. The effects of reinforcement, time duration and particle size on prepared samples of prepared composite were studied on slurry erosive wear. The static and accelerated corrosion tests were performed and the micro hardness of the developed composite was investigated. The experimental results on Al5083-Al<sub>2</sub>O<sub>3</sub>-Gr hybrid composite revealed that the addition of reinforcement improves the hardness and reduces corrosion and wear rate.

Sharanabasappa and Moti (2013) conducted a study on mechanical properties of fly ash and alumina reinforced aluminium alloy (LM25) composite. The mechanical properties of fly ash and alumina reinforced aluminium alloy composite samples, processed by stir casting were reported. It was found that the tensile strength and hardness of the aluminium alloy composite increased with the increase in percentage weight of Al<sub>2</sub>O<sub>3</sub>.

Daljeet *et al.* (2013) carried out an experimental investigation of mechanical behaviour by adding SiC and Alumina. Different percentages of SiC and Al<sub>2</sub>O<sub>3</sub> reinforcements were added and the behaviour of the composite were examined. It was concluded that the increment of the reinforcement increased the mechanical properties such as hardness, yield strength, and ultimate strength, but at the same time the behaviour of material changed from ductile to brittle.

Anilkumar *et al.* (2011) investigated the mechanical properties of fly ash reinforced aluminium alloy (Al6061) composite and found that, the tensile strength,

compressive strength and hardness of aluminium alloy (Al 6061) composite decreased with the increase in particle size of the reinforced fly ash. Increase in the weight fractions of the fly ash particles increased the ultimate tensile strength, compressive strength, hardness and decreased the ductility of the composite.

Denish and Jasmet (2014) carried out a comparative investigation of mechanical properties aluminium based hybrid metal matrix composite. The result indicated that there was an increase in the value of tensile strength, ultimate tensile strength, hardness value and flexural strength of newly developed composite, having SiC and B<sub>4</sub>C particulates in comparison to the SiC, graphite reinforced composite.

Veeresh *et al.* (2011) conducted a study on Al6061-SiC and Al7075-Al<sub>2</sub>O<sub>3</sub> metal matrix composite. Mechanical properties of the composite, such as hardness, tensile strength and wear resistance were presented. The SiC and Al<sub>2</sub>O<sub>3</sub> resulted to improving the hardness and density of the composite.

Asif *et al.* (2011) investigated the development of aluminium based hybrid metal matrix composite for heavy duty applications and investigated the dry sliding wear behaviour of aluminium alloy based composite, reinforced with silicon carbide particles and solid lubricants such as graphite antimony tri-sulphate (Sb<sub>2</sub>S<sub>3</sub>). The results revealed that, the wear rate of hybrid composite were lower than that of binary composite. The wear rate decreased with the increasing load, and increased with increasing speed.

Kesavulu *et al.* (2014) investigated the properties of aluminium fly ash metal matrix composite. Aluminium clad and fly ash chemical analysis were conducted before and after mixing and forming as particulate metal matrix composite, and comparing the mechanical and physical properties of the MMC at varying of fly ash addition.

Francis (2012) fabricated piston from aluminium scraps and aluminium-silicon were the material used. The cast piston was machined and subjected to performance rating test in a Jincheng AX100 motorcycle engine.

Venkateswara and Baswaraj (2014) tried with cast aluminium, aluminium MMC and brass to design the 5B.H.P diesel engine piston modelled in Pro/Engineer. Structural analysis was done on the piston by applying the pressure to verify the strength of the piston, using three materials. In a normal diesel engine, the amount of useful energy available is less, and the remaining is lost to the cooling water, exhaust gases and as frictional losses. The most effective way of burning various fuels in the engine and reducing the energy losses is by using thermal barrier coatings on the various elements of the combustion chamber, like cylinder head, cylinder liner, piston and valves.

Ajay and Pushpendra (2014) illustrated the procedure for analytical design of three aluminium alloy pistons, using specifications of four stroke single cylinder engine of Bajaj Kawasaki motorcycle. It was concluded from the results that the weight and volume of Al-GHS 1300 was least among the three materials. Hence, the inertia forces were less, which enhanced the performance of the engine. The FOS of Al-GHS 1300 is 6, much higher than the other materials, hence, further development of high power engine using this material is possible.

Rao and Raju (2014) studied the application of fly ash particle reinforcements on the microstructure, porosity and hardness in Al-(Si-Mg) cast composites. The fly ash reinforced composites were fabricated by the stir casting process and characterized by optical microscopy and hardness measurements. The results showed particle contents affect the porosity and hardness of the composites. An increase in the fly ash content

increase the porosity in the composites, with the matrix alloy reinforcement with 15wt% of fly ash particles having the highest porosity and lowest hardness.

Rohatgi *et al.* (2006) studied the application of fly ash in synthesizing low cost metal matrix composites for automotive and other engineering applications. The work summarized attempts of incorporating fly ash material content, cost and weight on selected industrial components while also improving selected properties.

Razzak *et al.* (2017) used Aluminium-fly ash (FA) particulate reinforced composites (AA6063-FA) in automotive and aerospace industries because of their low density and good mechanical properties. Three different weight fraction of FA: 2%, 4% and 6% were added to AA6063 alloy using compo casting method. The effect of FA particulates on microstructure, density and compression strength of AA6063- FA composites were investigated. Field Emission Scanning Electron Microscope (FESEM) micrographs revealed that the FA particulates were uniformly distributed in AA6063 alloy. The results also showed that density, compression strength and microstructure of the AA6063-FA composites are significantly influenced by the FA amount. The increase in the weight fraction of FA will improve the microstructure and enhance the compression strength. The density of AA6063-FA composites decreases as the incorporation of FA increases.

AbdulRahim *et al.* (2014) analysed a three dimensional flow of direct-injection diesel engine for different piston configuration, using computational fluid dynamics. Three-dimensional flow analysis of the intake, and compression stroke of a four valve direct-injection diesel engine were carried out with different combustion chambers. The three-dimensional model is reasonably accurate for crank angle around the top dead centre (TDC). In general, it performs better for low swirl combustion chambers, while

turbulence velocities are under predicted when squish effects are important. The flow characteristics inside the engine cylinder equipped with different piston configurations were studied. The results confirmed that the piston geometry had little influence on the (in-cylinder) flow during the intake stroke, and the first part of compression stroke. The bowl shape place a significant role at TDC and early stage of expansion stroke by controlling turbulent velocity field. The shapes are represented for the geometries usually employed for the optimum combustion chambers in real engines.

Venkata *et al.* (2013) analysed the stress distribution in the various parts of the piston to know the stresses due to the gas pressure and thermal variations, using ANSYS. Piston was designed, analysed and performance optimized using graphics software. The CATIAV5R16, CAD software for performing the design phase and ANSYS 11.0 for analysis and performance optimization phases were used. The volume of the piston was reduced by 24%, the thickness of barrel was reduced by 31%, width of other ring lands of the piston was reduced by 25%, Vonmises stress is increased by 16% and deflection was increased after optimization. But all the parameters were well within design consideration.

Sushma and Jagadeesha (2013) studied the effect of piston configurations on in-cylinder flow, where a single cylinder direct injection diesel engine was used. For obtaining swirl intensity, helical-spiral combination inlet manifold were used. Increase in swirl intensity resulted in better mixing of fuel and air. Swirl velocities in the charge can be substantially increased during compression by suitable design of the piston. The effect of different piston configuration on air motion and turbulence inside the cylinder of a Direct Injection (DI) diesel engine was carried out, using Computational Fluid Dynamics (CFD) code.

Ismail *et al.* (2009) worked on the design and analysis of piston head through reversed engineering. Piston head of existing car component was selected and measured using coordinates. Chemical composition of the piston head was taken by chemical test, and the piston was modelled. The simulation was carried out for different material, to find out the better chemical composition to make a new piston head.

Ayatollahi *et al.* (2011) carried out a precise finite element method (FEA), in order to attain its high cycle fatigue (HCF) safety factor, and low cycle fatigue (LCF) life. The piston was subjected to non-proportional multi-axial loading. The non-proportional loading led to an additional cyclic hardening in the material, and the relative stress gradient parameter was used in order to perceive stress concentration and notch effect.

Bhattacharya (2014) investigated and analysed the stress distribution of the piston at the actual engine condition during combustion process. The parameters used for the simulation were operating gas pressure and material properties of piston. The piston was modelled in CATIA software and analysed using ANSYS workbench.

Franz and Seshasai (2009) conducted a research on CFD-based optimization of fuel injection strategies in a diesel engine, using an adaptive gradient method. A gradient-based optimization tool has been developed and, in conjunction with a CFD code, utilized in the search of new optimal fuel injection strategies. The approach taken used a steepest descent method, with an adaptive cost function, where the line search is performed with a back tracking algorithm. The back tracking algorithm utilizes quadratic and cubic polynomials to accelerate the convergence, and the initial back tracking step employs an adaptive step size mechanism, which depends on the steepness of the search direction.

Ibrahim *et al.* (2008) investigated the Cylinder In-Flow through Piston-Port Engines Modelling using Dynamic Mesh. They presented numerical study of three-dimensional analysis of two-stroke spark-ignition (SI) cross loop-scavenged port. The objective of their study was to investigate the in-cylinder characteristics at motored transient condition. The pressure on in-cylinder and intake port were collected and applied for validation with numerical results for 1400 rpm. The three-dimensional modelling analysis was performed utilizing dynamic mesh method. The prediction of distribution of in-cylinder pressure and mass fraction of gases function of crank angle were investigated. The results showed that the relative error between experimental and numerical was less than 2 %.

Silva *et al.* (2013) compared a circular piston with a square shaped piston (piston with square-shaped crown). In this comparison, the focus was mainly on mechanical parameters like stress induced, strain induced and deformation of the piston. From the analysis, it can be seen that for some instances, a square piston is better in terms of the total deformation, equivalent stress and maximum principle stress, without considering friction and other losses. Although it might seem better to use a square shaped piston head instead of a circular shaped one, after looking at these results, but it will require extra cooling arrangements and more maintenance.

Venkatesh and Viveknanda (2014) developed a manufacturing process plan for aerospace piston ring which is used in rockets using computer aided manufacture (CAM), (NX 7.5), which is exclusively CAM software, used to generate part program by feeding the geometry of the component and defining the proper tool path, and thus, transferring the generated part program to the required CNC machine with the help of DNC lines. These piston rings are used to release the rocket due to the pressure release in the chamber. The

operator thus executed the program with suitable requirements. Two different manufacturing process plans were developed, using NX-CAM software and the optimum process plan were determined with less machining time and improved surface finish.

Khaleel *et al.* (2016) built a simulation model of new manufacturing system for new plant to produce 1200 engine components per day. The system was flexible, reliable and within maximum scrap rate of 1%. Furthermore, the optimization and analysis of production performance measures, which are inclusive of cost, machine utilizations, and jobs per hour, helped the company studying the system, and selecting optimal scenario, as well as to support upper management to make perfect decision before implementing a new system.

Kethavath *et al.* (2015) modelled and assembled piston with the help of CATIA software. The component was meshed and analysed using ANSYS software, and the thermal and static behaviour was studied and the results were tabulated. The various stresses acting on the piston under various loading conditions were identified.

Chanthni and Mevan (2015) carried out a physicochemical analysis of coconut shell powder. Laser diffraction was used to determine the distribution and the mean particle size of 34.2 microns. Variety of sizes, shapes and structures were identified, using electron microscopy. The chemical composition, lignin content of the coconut shell particle was estimated. The ash content and types of metal were determined. Apart from silica which could not be measured, sodium, potassium, zinc, calcium and iron were found to be the metals. Steel or ceramic cast-in elements were used as local reinforcements to improve the high temperature mechanical properties and/or to control thermal expansion (that is, reduce the effects of different thermal expansion coefficients



in contact areas with other materials). (European Aluminium Association, Automobile Manual, 2015).

Deborah (2019) carried out a research on carbon composites. It was revealed from the research that, metal-matrix composites with discontinuous or continuous carbon fibres or carbon nanotubes (CNTs) are attractive for the thermal conductivity of the metal matrix, the low coefficient of thermal expansion (CTE), high thermal conductivity, and high elastic modulus of the fibrous carbon. The combination of high thermal conductivity and low CTE is valuable for heat sinks and other components in microelectronic packaging. In addition, the fibrous carbon enhances the lubricity and wear resistance. Methods of composite fabrication include liquid metal infiltration, powder metallurgy, and stir casting. Due to the reactivity of liquid metals with carbon to form carbides and the inadequate wetting of the fibrous carbon by liquid metals, the coating of the fibrous carbon is commonly conducted prior to composite fabrication. The coatings include metals and ceramics. Common metal matrices for structural applications include aluminium, magnesium, copper, and titanium. For soldering and brazing, tin-matrix and silver-matrix composites are relevant. The processing, structure, and properties of metal-matrix composites are covered.

Kinshawy (2019) worked on Machining Technology for Composite Materials. It was reported from the research that Metal matrix composite materials (MMCs) offer various mechanical properties that are not offered by conventional unreinforced monolithic metal counterparts; specifically, high temperature stability, specific strength, and wear resistance. As a result, these composite materials have different applications in several industries including automotive and aerospace. However, machining of MMCs still remains a challenge. Understanding the manufacturing methods, strengthening

mechanisms and hence mechanical properties of MMCs is crucial to comprehension of their deformation behaviour during machining and the resulting workpiece surface integrity and tool wear. The chapter described the types of composites and their unique physical properties. In addition, the cutting performance of some composite materials were discussed.

Bello *et al.* (2015) investigated the possibility of using mechanical milling for the synthesis of un-carbonised coconut shell nanoparticles (UCSNPs). UCSNPs were synthesized from discarded coconut shells (CSs) using top down approach. The sundried CSs were crushed, ground and then sieved using hammer crusher, a two disc grinder and set of sieves with shine shaker respectively. The CS powders retained in the pan below 37  $\mu\text{m}$  sized sieve were milled for 70 hours to obtain UCSNPs. Samples for analysis were taken at 16 and 70 hours. UCSNPs were analysed using transmission electron microscope (TEM), scanning electron microscope (SEM) with attached EDS and Gwydion software. Samples of UCSNPs obtained at 16 and 70 hours showed that the deep brown colour of the initial CS powder became fading as the milling hour increased. The size determination from TEM image revealed spherical particles with an average size of 18.23 nm for UCSNPs obtained at 70 hour milling. The EDS spectrographs revealed an increase in the carbon counts with increased milling hours. This was attributable to dryness of the CS powders by the generated heat during the milling process due to absorption of kinetic energy by the CS powders from the milling balls. SEM micrographs revealed UCSNPs in agglomerated networks. The SEM micrograph/Gwydion particles size determination showed average particles of  $170.5 \pm 3$  and  $104.9 \pm 4.1$  nm for UCSNPs obtained at 16 and 70 hours respectively. Therefore, production of UCSNPs through mechanical milling using mixture of ceramic balls of different sizes has been established especially when the particles of the sourced/initial CS powders falls below 37  $\mu\text{m}$ .

Vinod and Mittal (2013) illustrate design procedure for a piston for 4 stroke petrol engine for hero bike and its analysis by its comparison with original piston dimensions used in bike. The design procedure involved determination of various piston dimensions using analytical method under maximum power condition. The research considered combined effects of mechanical and thermal loads while determining various dimensions. The basic data of the engine were taken from a located engine type of hero bike. The work provided a fast procedure to design a piston which can be further improved by the use of various software and methods. The most important part was that, very less time was required to design the piston with only a few basic specification of the engine.

Meta-analysis is a set of techniques used “to combine the results of a number of different reports into one report to create a single, more precise estimate of an effect”. The aims of meta-analysis are “to increase statistical power; to deal with controversy when individual studies disagree; to improve estimates of size of effect, and to answer new questions not previously posed in component studies” (Julien, 2015). Table 2.5 shows meta-analysis of selected literature

**Table 2.5 Meta-Analysis of Selected Literature**

<b>Author/Year</b>	<b>Title</b>	<b>Contribution</b>	<b>Limitations</b>
1. (Pardeep <i>et al.</i> , 2016)	Effect of graphite reinforcement on physical and mechanical properties of aluminum metal matrix composites	The use of graphite reinforcement in Aluminium matrix	1. Lack of wet ability between aluminium and the reinforcement 2. Oxidation of the Graphite lead to manufacturing difficulties and cavitation of the material at high temperature
2. (Ogbonnaya, <i>et a.</i> , 2013)	Development of CNC Program for Piston Production	The use of Aluminium scraps to produce piston using CNC	Characterization of aluminium scraps was not carried out.
3. (Chanthni and Mevan, 2015)	A physico-Chemical analysis of coconut shell powder	The research characterized and analysed coconut shell powder for better understanding of its properties.	The work was to determine the physical and chemical properties of coconut shell powder.
4. (Razzak <i>et a.</i> , 2017)	Microstructural Characterization of fly ash Particulate Reinforced AA6063 Aluminium Alloy for Aerospace Application	Investigation of the effect of fly ash particulate on microstructure, density and compression strength of AA6063-FA composites.	The study was on fly ash and aluminium AA6063.

<b>Author/Year</b>	<b>Title</b>	<b>Contribution</b>	<b>Limitations</b>
5. (Silva <i>et al.</i> , 2013)	Design Analysis of A Circular and A Square Shaped Piston Head Considering Mechanical Stress Induced	Using Autodesk Inventor, the two shapes were compared and circular piston was proposed in preference to square piston.	The outcome was limited to the capabilities of the software used.
6. (Monikandan <i>et al.</i> , 2016)	Dry sliding wear studies of aluminium matrix hybrid composite	Hybrid composite of aluminium with %B4C-MOS2 was produced.	The study was on fly ash and aluminium AA6063.  The review was on coconut fibre, not particle reinforcement. Coconut fibre has lower working temperature when compared to coconut particle reinforcement
7. (Udhayasankar and Karthikeyan, 2015)	International Journal of Chem- Tech Research	Review on Coconut shell reinforced composites	The aerospace component was piston ring used in rockets.
8. Ventakash and	Structural Analysis and	Machining process	

Author/Year	Title	Contribution	Limitations
Viveknanda, (2014)	Manufacturing Process Optimization of an Aerospace Component	plan of piston ring using CAM (NX 7.5) with less machining time and more surface finished was achieved.	The research was limited to machining of metal matrix composite
9. (DilipKumar and Madhura, 2015)	Theoretical Analysis of stress and design of piston head using CATIA and ANSYS	Analysis of thermal stresses and damages due to application of pressure and comparison was made to find a suitable design	.
(Kinshawy, 2019)	Turning Processes for Metal Matrix Composite.	The deformation behaviour of metal matrix composites during machining operation was investigated.	

## **2.6 Research Gap**

The use of coconut shell ash as a reinforcement of Aluminium metal composite for a car engine piston production. From literature reviewed so far, the use of this local material has not been explored, particularly in the production of piston.

## CHAPTER THREE

### 3.0 MATERIALS AND METHODS

#### 3.1 Materials and Equipment

In addition to the piston design, material is a major element in the piston manufacturing. The common materials that are always used in the manufacture of pistons are aluminium and cast iron. Nowadays, pistons are made using aluminium alloy as the raw material, compared to cast iron in the early manufacturing of pistons. Earlier, low speed engine also had pistons of cast iron to match the material used for the cylinder. (Kethvath *et al*, 2015)

##### 3.1.1 Materials

The materials used in the research work were:

- I. Coconut shell (Collected in Kaduna State)
- II. Aluminium alloy 356-T7: JODA CO. LTD China
- III. Hexachloroethane: Sourced in Kaduna
- IV. Magnesium: Sourced in Kaduna
- V. Stainless Steel: Sourced in Kaduna
- VI. Casting Sand: Foundry Workshop Kaduna Polytechnic

##### 3.1.2 Equipment and Tools

These are categorized into two;

- a) Equipment and Tools for Composite preparation and testing
  - I. Electric Resistance Furnace: spark industry (Henan) CO. LTD, China Model:STD-640-12
  - II. Graphite Crucible Furnace: Hebei Zhuli Carbon CO. LTD China:Model: 8T-60T



- III. Hammer Crusher: Zhili Wear Parts, 1818 bi-Metal Crusher Hammer, China
- IV. Transmission Electron Microscope, JEOL model: JSM-6510 LV series
- V. Rockwell Hardness Tester, Model 38506, USA
- VI. Set of Sieves with a Sine Shaker: S20 (VD 30), Russia
- VII. En-32 steel hardened Pin-On-Disc
- VIII. Casting Mould: Wuxi Yongjie Machinery Casting CO. LTD, China
- IX. TGA Q50 thermogravimetric analyser

**b) Equipment and Tools for Piston Machining**

- I. Harrison M300 Colchester Lathe Machine, USA
- II. Radial Arm Drilling Machine, Gate: Model: WR 50/2, USA
- III. Boring Machine, LBM: Model: 250 USA
- IV. Reamers: RKE-01S, Kenna Metal CO. LTD, USA

### **3.2.0 Methods**

#### **3.2.1 Production of Coconut Shell Ash**

Coconut shell was ground to form coconut shell powder, the powder was packed in a graphite crucible and fired in an electric resistance furnace at a temperature of 1300<sup>0</sup>C to form the coconut shell ash (CSAp), Plate III and IV.



**Plate III: (a) Crushed**



**(b) Ground Coconut Shell**



**Plate IV: (a) Coconut Shell Powder**

**(b) Coconut Shell Ash**

### **3.2.2 Particle Size Analysis**

The coconut shells were dried under the sun for two months, after which they were broken into smaller pieces with the aid of hammer crusher. The crushed coconut shell pieces were ground, using a two disc grinder to obtain the powder. The powder was packed in a graphite crucible, and fired in an electric resistance furnace at a temperature of 900<sup>0</sup>C, to form the coconut shell ash (CSAp), which were sorted into different sizes, arranged in descending order of grain fineness number. The sieves were shaken for fifteen minutes, using a sine shaker. The sieves sizes ranged from 355-63 $\mu$ m. The coconut shell powders retained in the pan below 70 $\mu$ m, were used for the analysis, in line with the work of Bello *et al.* (2015). The morphology and particle size analyses were carried out, using transmission electron microscope (TEM) scan. The particle size analysis of the coconut shell ash particles was carried out in accordance with BS1377:1990 (Nijssen, 2015).

### **3.2.3 Thermal Analysis**

Thermal composition (TA) was observed in terms of global mass loss by using a TA instrument TGA Q50 thermogravimetric analyser. The apparatus detected the mass lost with a resolution of 0.1 as a function of temperature. The sample were evenly and loosely distributed in an open sample pan of 6.4mm diameter and 3.2mm deep with an initial sample weight of 8-

10 mg. The temperature change was controlled from room temperature ( $25\pm 3^{\circ}\text{C}$ ) to  $900^{\circ}\text{C}$  at a heating rate  $10^{\circ}\text{C}/\text{min}$ .

High purity argon was continuously passed into the furnace at a flow rate of 60ml/min at room temperature and atmospheric pressure. Before the start of each run, the argon was used to purge the furnace for thirty minutes to establish an inert environment in order to prevent any unwanted oxidative decomposition. The TG and DTA curves were obtained using universal analysis 2000 software from TA instrument.

### **3.2.4 Density Measurement**

Density measurements were carried out on the coconut ash and composite samples using Archimedes' principle. The buoyant force on the submerged object is equal to the weight of the fluid displaced. This principle is useful for determining the volume and therefore the density of an irregular shaped object, by measuring its mass in air and its effective mass when submerged in water (density = 1 gram/cc). This effective mass under water was its actual mass minus the mass of the fluid displaced. The difference between the real and effective mass therefore gives the mass of the water displaced, and allows the calculation of the volume of the irregular shaped object. The mass divided by the volume thus gives a measure of the average density of the samples.

### **3.2.5 Hardness Test**

The hardness values of the samples were determined according to ASTM E18-103, (2000) using the Rockwell hardness tester on "B" scale, with a 1.56mm steel ball indenter, minor load of 10kg, and major load of 100kg and hardness value of 101.2HRB on the standard block. Before the test, the mating surfaces of the indenter, plunger rod and test samples were thoroughly cleaned by removing dirt, scratches and oil, and calibration of the testing machine using the standard block. The samples were placed on an anvil, which acts as support for the

test samples. A minor load of 10kg was applied to the sample in a controlled manner without inducing impact or vibration, and zero datum position was established. The major load of 100kg was then applied. The reading was taken when the large pointer came to rest or had slowed appreciably and dwelled for two seconds. The load was then removed by returning the crank handle to the latched position and the hardness value read directly from the semi-automatic digital scale.

### **3.2.6 Tensile Test**

The tensile test on the samples were conducted Tinus-Olsen tensile testing machine at a strain rate of  $2 \times 10^{-3} \text{s}^{-1}$ . The test pieces were machined to the standard shape and dimensions as specified by the American Society for Testing and Materials (ASTM D, 2000). The sample was locked securely in the grips of the upper and lower jaws, and then the load was increased until failure occurred. The values of the load and the extension were recorded and were used in obtaining the stress-strain graph.

### **3.2.7 Wear Test:**

A pin-on-disc test apparatus was proposed to investigate the dry sliding wear characteristic of the composite, according to ASTM G99-95 Standards (Monikandan et al 2016). The disc to be used was an En-32 steel hardened to 62 HRE, 120mm track diameter and 8mm thick, with surface roughness of  $101 \mu\text{m}$ . The initial weight of the samples was measured, using a single pan electronic weighing machine with accuracy of 0.01g. During the test, the pin was pressed against the rotating disc. The wear tests was conducted by varying applied load from 10 to 15N at a constant speed of 2.0m/s and sliding distance of 400mm. The wear of the samples investigated is a function of the percentage volume of reinforcement, applied load and sliding velocity. The formula used to convert the weight loss into wear rate (WR) is given as:

$$WR = \frac{\Delta w}{s} \quad 3.1$$

Where,  $\Delta w$  is the weight difference of the sample before and after the test,  $s$  is the total sliding distance.

### 3.2.8 Determination of Coefficient of Friction

A measuring scale was used to measure the perpendicular forces acting on the sample and the resistive forces by the sample. The varied load from 10 to 50N at an interval of 10N were applied to the sample with varied weight of coconut shells as reinforcement from 3 to 15wt% at an interval of 3wt% and were made to slide on the sliding platform of the measuring scale. The resistive forces as well as the perpendicular forces were read off from the scale. The coefficient of friction,  $\mu$ , was then calculated using equation 3.2 according to Keneth et al. (2014) as:

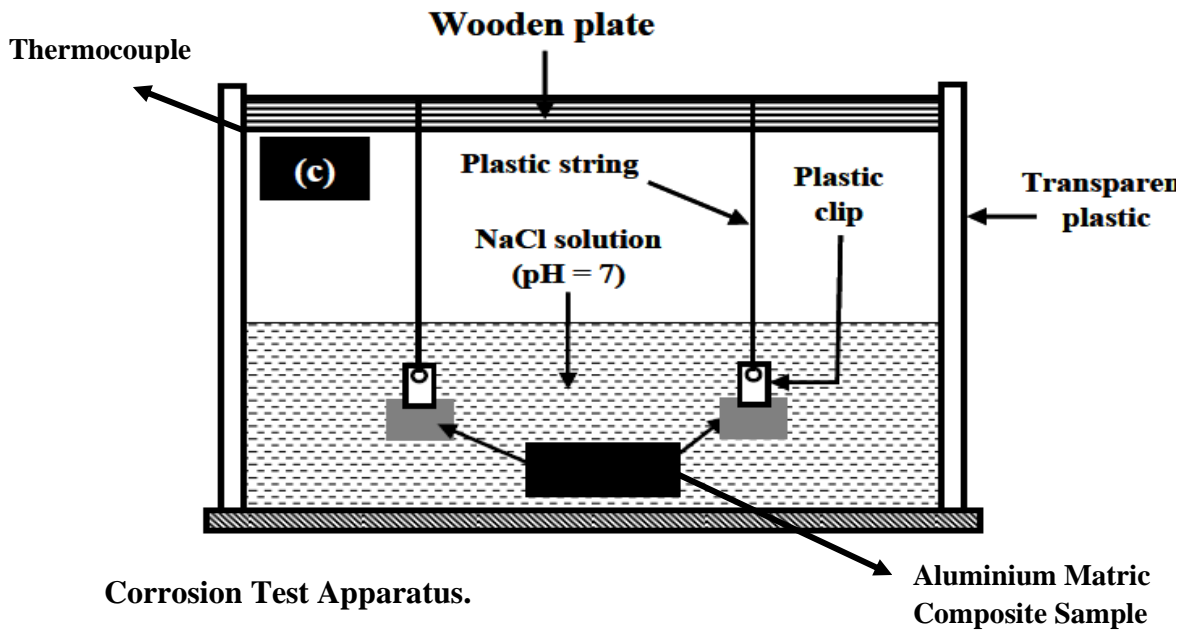
$$\mu = F_r / N \quad 3.2$$

Where  $F_r$  is the resistive force,  $\mu$  is the coefficient of friction,  $N$  is the perpendicular force.

### 3.2.9 Corrosion Test

The standard immersion corrosion test was used to investigate the weight loss and corrosion rates of the composite materials in specified electrolytes. Test samples were polished using several grades of emery paper ranging from 240 to 600 grit, rinsed in distilled water and methanol, and dried, then weighed using an electronic weighing balance. The sample weights were measured in grams to 4 decimal places. After weighing, the samples were immersed in 3.5 wt. % NaCl solution. The plastic threads were attached to a wooden support as shown in Figure 3.1 and the solution-to-sample surface area ratio was  $312.5 \text{ ml cm}^{-2}$ . After each immersion test, the samples were extracted from the electrolyte and cleaned in 70 wt. %  $\text{HNO}_3$  (specific gravity = 1.4134) for 1 to 5 minutes as specified by ASTM G1 (Oloruntoba *et al.*, 2015). The exposure time was varied from 1, 3, 6, 9, 12, and 15 days (giving a cumulative

total exposure time of 46 days for each sample). The corrosion products on the surface of the samples were removed by rubbing gently against a soft wet nylon sponge drenched in water. The specimens were then cleaned in methanol.



The samples were placed in an air furnace maintained at 100°C for 2 hours and subsequently cooled to room temperature at the rate of 0.625°C/min and re-weighed. The cleaning procedure was observed after each exposure. To account for metal loss resulting from cleaning of the samples, the weight loss of un-corroded control sample was obtained using the same cleaning procedure. Weight loss data were obtained by subtracting weights obtained after each exposure to the electrolyte from the initial weights before the exposure. The corrosion rate of each sample in mm/year was determined using the expression of equation 3.3:

$$Mm/yr = 87.6 W / DA\tau \tag{3.3}$$

Where  $W$  is the weight loss in mg,  $D$  is density in g/cm<sup>3</sup>,  $A$  is surface area in cm<sup>2</sup>, and  $\tau$  is time in hours (Orhororo *et al.*, 2017).

### 3.3 Design Analysis and Calculation of Piston Parameters

The engine used for this work is a 4 cylinder four stroke TOYOTA, model 12V petrol engine.

The engine specifications are given in Table 3.1.

**Table 3.1 Engine Specifications**

PARAMETERS	SYMBOLS	VALUES
Engine Type		Four stroke, petrol engine
Number of cylinders		4 cylinders
Bore Diameter	D	72.0mm
Piston Stroke	↓	77.4mm
Displacement volume	X	1295 cc
Compression ratio	CR	9.5/1
Maximum power	P	74 Kw
Maximum torque	T	117N-m
Number of revolutions/cycle	N	800 rpm

Source: Budynas & Nisbett (2014)

#### 3.3.1 Determination of Thickness of the Sealing Part of the Piston

The thickness ( $s$ ) of the sealing part is given according to Prasad *et al.* (2016) is given as:

$$s = 0.05 \times D \quad 3.4$$

Therefore:  $s = 0.05 \times 72 = 3.6mm$

#### 3.3.2 Estimation of the Piston Crown Radius

The crown inner radius ( $r_i$ ), is given according to Dilipkumar and Madhura, (2015) as:

$$r_i = D/2 - (s + t + dt) \quad 3.5$$

Where D is the bore diameter given as 72mm, as shown in Table 3.1. For this diameter the radial thickness (t) and the radial clearance (dt) are 3 and 0.08mm respectively.

(Venkata *et al.*, 2013)

$$r_1 = 72/2 - (3.6 + 3 + 0.8) = 28.6mm$$

### 3.3.3 Determination of Stress Acting on the Piston Crown

The stress ( $\sigma_b$ ) acting on the piston crown according to Jadhav *et al.* (2015) is given as:

$$\sigma_b = \frac{M_b}{W_b} = P_{zmax} (r_i/\delta)^2 \quad 3.6$$

where  $\delta$  = thickness of the piston crown, given as:

$$\delta = dt \times D = 0.08 \times 72 = 5.67 \approx 6mm$$

$$p_{zmax} = 2MPa$$

$$\sigma_b = 2(28.6/6)^2 = 45.50MPa$$

### 3.3.4 Determination of Angular Velocity of the Piston

The angular velocity ( $\omega$ ) of the piston is given according to Venkata *et al.* (2013) as:

$$\omega = \frac{2\pi \times rpm}{60} \quad 3.7$$

The engine rpm is given in Table 3.1 as 800rpm

$$t = 1/800 \text{ min or } t = 0.00125 \text{ sec}$$

$$\text{Therefore, } \omega = 2 \times 3.142 \times \frac{800}{60} = 83.775 \text{ rad/sec} \approx 83.8 \text{ rad/sec}$$

### 3.3.5 Determination of Linear Velocity of the Piston

The linear velocity, according to Khurmi and Gupta, (2004) is given as:



$$\text{Linear Velocity} = \text{Angular Velocity} \times \text{radius} = 83.775 \times 36$$

$$\text{Linear Velocity} = 3016.8 \text{ mm/s}$$

### 3.3.6 Determination of the piston head thickness

The piston head thickness ( $t_H$ ) is calculated using Grashoff's formula, according to Sandeep and Vishnu, (2005) as:

$$t_H = \sqrt{\frac{(3pD^2)}{(16\sigma_t)}} \text{ mm} \quad 3.8$$

where

$p$  = maximum pressure in N/mm

$D$  = cylinder bore/outside diameter of the piston in mm.

$\sigma_t$  = permissible tensile stress for the material of the piston.

Permissible tensile stress for the material of the piston:

Here the material is a particular grade of AL-Si alloy whose permissible stress is 50 Mpa-90MPa. However the permissible stress of 90MPa was used.

Before calculating thickness of piston head, the diameter of the piston has to be specified.

The piston size that has been considered has an L×D, specified as 73.5×72, where L is the length of the piston, Factor of safety (F.O.S) According to Khurmi and Gupta, (2004) is given as 1.2.

Therefore;

$$\sigma_t = \frac{\sigma_p}{F.O.S} = \frac{90}{1.2} = 75 \text{ MPa}$$

The maximum pressure experienced by the piston, according to Venkata *et al.* (2013) is between 1.4 and 1.8MPa, however, the pressure of 1.4MPa was used.

Using equation 3.8:

$$t_H = \sqrt{(3 \times 1.4 \times 72^2) / (16 \times 75)}$$

$$t_H = 4.2 \approx 4mm$$

### 3.3.7 Analysis of Piston Rings:

The radial width ( $b$ ) of the piston, is given according Budynas and Nisbett, (2014), as:

$$b = D \sqrt{3p_w} / \sigma_t \quad 3.9$$

Let the radial thickness of ring  $b = (t_1)$

Where  $D =$  cylinder bore in mm

$P_w =$  pressure of fuel on cylinder wall in N/mm<sup>2</sup>. Its value is limited from 0.025N/mm<sup>2</sup> to 0.042N/mm<sup>2</sup> according to venkata *et al.* (2013). For present material,  $\sigma_t$  is 90Mpa

$$t_1 = 72\sqrt{3 \times 0.042} / 90 = 2.69mm$$

### 3.3.8 Determination of the Minimum Axial Thickness of the Piston Rings

The Minimum axial thickness, according to venkata *et al.* (2013) is given as:

$$t_2 = D / (10 \times n_r) \quad 3.10$$

Where  $n_r =$  number of rings

$$t_2 = 72 / (10 \times 3) = 2.4mm$$

The thickness of the rings according to Prasad *et al.* (2016) is given as:

$$t_2 = (0.7b \text{ to } b) = 0.7 \times 2.69 = 1.883 \text{ mm}$$

Width of Top Land and Ring Lands: The width of the top land varies from

$$b_1 = t_H \text{ to } 1.2 t_H$$

Width of top land:

$$b = t_H \text{ to } 1.2t_H = 1.2 \times 4.2 = 5.04mm$$

Width of other lands ( $b_2$ )

Width of other ring lands varies from

$$b_2 = 0.75t_2 \text{ to } t_2 \quad b_2 = t_2 \text{ to } 0.75t_2 = 0.75 \times 2.4 = 1.8mm$$

### 3.3.9 Analysis of the Piston Barrel (skirt):

The maximum thickness of piston barrel ( $t_3$ ), is given according to Jadhav *et al.* (2016) as:

$$t_3 = 0.03 \times D + b + 4.5mm \quad 3.11$$

Where

$b$  = Radial depth of piston ring groove (Radial width of the piston)

Thickness of piston barrel ( $t_3$ ) at the top end is given as:

$$t_3 = 0.03 \times 72 + 2.69 + 4.5 = 9.35mm$$

According to Sandeep and Vishnu, (2015), the thickness of the piston barrel and length of skirt, are calculated as:

Thickness of piston barrel at the open end:

$$t_2 = (0.25t_3 \text{ to } 0.35t_3)$$

$$t_2 = 0.35 \times 9.35 = 3.27 \text{ mm}$$

Length of the skirt ( $l_s$ ) is given as:

$$l_s = (0.6 D \text{ to } 0.8 D)$$

$$l_s = 0.8 \times 72 = 57.6 \text{ mm}$$

### **3.3.10 Determination of length of piston pin in the connecting rod bushing**

Length of piston pin ( $l_1$ ) in the connecting rod bushing is calculated according to Manish *et al.* (2016) as:

$l_1 = 45\%$  of the piston diameter

$$l_1 = 0.45 \times 72 = 32.4 \text{ mm}$$

### **3.3.11 Determination of piston pin diameter**

Piston pin diameter according to Manish *et al.* (2016) is given as:

$$d_o = (0.28 D \text{ to } 0.38 D)$$

$$d_o = 0.38 \times 72 = 27.36 \text{ mm}$$

The centre of the piston pin should be  $0.02 D$  to  $0.04D$  above the centre of the skirt

Thus, the dimensions for the piston are calculated and these are used for modelling the piston.

In the above procedure, the ribs in the piston are not taken into consideration, so as to make the piston model simple in its design, that is, one faced. In modelling a piston, considering all factors will become tedious process. Thus, a symmetric model is developed using the above dimensions approximately.

### 3.4 Composite Preparation using Stir Casting

The production of the composites was done by the double stir-casting method. Initially, Al-7% weight of alloy was charged into the graphite crucible furnace and heated to about 750<sup>0</sup>C, till the entire alloy in the crucible was melted and 2% by weight of iron powder was added. The reinforcement particles (CSA) were preheated to 800<sup>0</sup>C for one hour, before incorporation into the melt. After the metal was fully melted, 0.05wt% degassing tablets (hexachloroethane) were added to reduce the porosity. Simultaneously, 1% by weight of magnesium was added to the melt in order to enhance the wettability between coconut shell ash particles and the alloy melt. It was noticed that without the addition of magnesium, the particles of coconut shell ash were rejected. The stirrer made of stainless steel was lowered into the melt slowly to stir the molten metal during the stirring time. The stirring rate continued for another five minutes, even after the completion of particle feeding. The mixture was poured into the mould which was also preheated in an oven until the molten metal was ready for pouring (Callister, 2013). Using this process, the cast piston was produced with 0, 3, 6, 9, 12 and 15%W CSA particle reinforced composites. A cast composite pistons were produced, as shown in Plate V.



**Plate V: Cast Composite Piston**

### 3.5 Piston Machining Process

The process flowchart for the machining of piston is presented in Figure 3.2

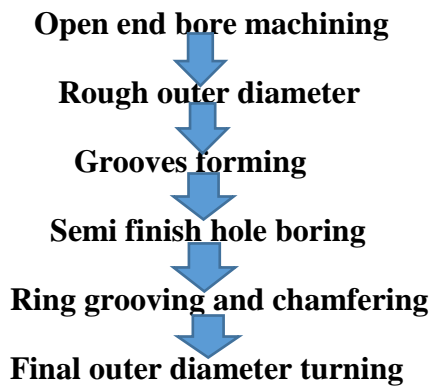


**Figure 3.2 Flow Chart for Piston Machining**

Machining process involves the following steps:

Open end bore machining

Rough outer diameter turning

Grooves forming

Semi finish hole boring

Cyclic grooving oil hole drilling in third groove and skirt

Ring grooving and chamfering: Final outer diameter turning: De-burring and cleaning

Tin coating

Finish pin hole boring

#### 3.5.1 Pinhole Boring

At this stage of the piston manufacturing process, the casting has the gudgeoned pin hole rough machined. This was carried out on a lathe machine specified under 3.1.2.

The pin borer was only a rough machining process which allowed the reamer to enter the gudgeoned hole later.

### **3.5.2 Turning**

Turning of the casting was carried out on the lathe machine.

This equipment is the most accurate and fastest available for this application with very tight tolerances and fast spindle speeds range of 200- 300rpm.

Workpiece was fixed between the spindle and the tailstock, an electric motor brought it to a constant rotational speed and it was processed using tools. All lathes have the same structure, namely the bed, the frame, the main spindle, the drive system and the carriage. The differences concern, amongst others, the turning diameter, and the spindle bore, the distance between centres and the machine weight.

The following operations were performed on this machine:

- Open end bore machining
- Rough outer diameter turning: Grooves forming

### **3.5.3 Drilling and Grinding**

Drilling included all oil holes in places such as the gudgeoned pin bosses and oil ring grooves.

Slotting was done where slots were placed in the skirt or in the oil ring groove. Surface speed, surface footage, and surface area are all directly related. If two tools of different sizes are turning at the same revolutions per minute, the larger tool has a greater surface speed. Surface speed is measured in surface metre per minute. All cutting tools work on the surface footage principle. Cutting speeds depend primarily on the kind of material to be cut, and the kind of cutting tool you are using. The hardness of the work material has a great deal to do with the recommended cutting speed. The harder the work material, the slower the cutting speed. The softer the work material, the faster the recommended cutting speed

$$RPM = CS \times 4 / D_c \quad 3.12$$

Where CS, is the cutting speed, 300

$D_c$ , is the diameter of the cutter = 0.5mm

$$RPM = 300 \times 4 / 0.5 = 2400rpm$$

Table feed ( $V_f$ ) is expressed according to Miltiadis, (2010) as:  $V_f = n \times f_z \times z$  3.11

Where:  $n$  = RPM,  $f_z$  = recommended feed, given as 0.15 mm/tooth from cutting tools catalogue and  $z$  = number of cutting tool teeth.

$$V_f = 2400 \times 0.15 \times 6 = 2160mm/min$$

Grinding involved the final size being machined on the piston: Semi-finish hole-boring: Circlip grooving, oil-hole drilling in third groove, and skirt ring grooving and chamfering

### 3.5.4 Deburring and Tin Coating

Before coating, the pistons were thoroughly cleaned to remove any soap or phosphate residue, water spots, machining oil, and dirt picked up during the manufacturing process. For optimum results, a mechanical type cleaner (spray) is recommended. Recommended methods for applying Tin Coating to pistons are either screen print or spray techniques.

**3.5.5 Reaming:** The final machining process for the piston was that of reaming. This process involved the piston being placed in a bath of oil and reamed at different sizes to reach the final size required. Since the pin boring process was only rough it was necessary to ream the pin bore a number of times to achieve the surface finish and size required.



### 3.6 Calculating RPM for Reaming

The drill press RPM setting for reaming depends on the cutting speed of the material and the size of the ream. The RPM setting will change with the size of the ream. As the ream got smaller, the RPM was increased to maintain the recommended surface footage. Although specific cutting speeds for reaming are available, a simple rule of half the speed was used for reaming operations. Using half the spindle speed for the drilling operation is a commonly accepted method for determining the reaming speed in most machine shops. RPM for reamer is expressed by Mitiadis, (2010) as

$$RPM = \frac{\text{spindle speed for drilling operation}}{2} \quad 3.13$$

$$RPM \text{ for reamer} = \frac{2400}{2} = 1200rpm$$

### 3.7.0 Performance Test on the Piston

#### 3.7.1 Idle and low speed engine performance test experiment, using MMC piston

A Toyota Model 12 valve engine, shown in Plate VI, was used in carrying out the performance test. The engine was assembled, serviced and then test run to determine performance and effectiveness of the engine. Fuel of about 100ml was discharged into the fuel chamber using the conventional and AMCs piston, then the engine was allowed to run until the fuel in the chamber was consumed.

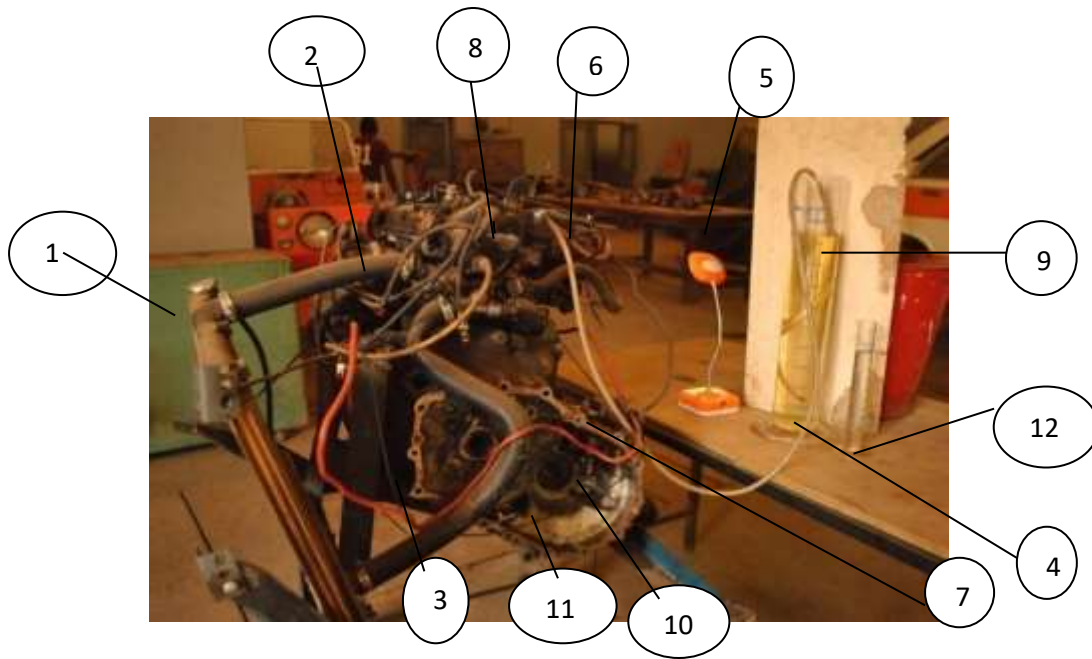


**Plate VI: Photograph Toyota Model 12 valve engine.**

(Automotive Laboratory, Kaduna Polytechnic, 2019)

In Table 4.12 Some parts of the Toyota Model 12 valve engine are:

1. Radiator
2. Radiator upper hose
3. Radiator lower hose
4. Petrol hose connect to fuel pump
5. Petrol hose connect to carburator
6. Kick starter
7. Clutch housing
8. Distributor with high tension cable
9. Graduation cylinder
10. Exhaust pipe end
11. Engine Test Rig
12. Graduation cylinder table

This was followed by 200ml (0.2litres) of fuel using a calibrated glass measuring cylinder which was discharged into the engine and allowed to run.

Finally, 300ml (0.3litres) of fuel was again discharged into the engine through the same channel and the engine was allowed to run. The durations of fuel consumption were recorded.

The consumption per kilowatt hour of the produced aluminium matrix composite and the conventional standard piston, according to Kesavulu *et al.* (2014) is given as:

$$\text{fuel consumption} / \text{KWh} = \frac{\text{vol.of fuel in litres}}{\text{time taken to consume fuel} \times \text{kw}} \quad 3.14$$

## CHAPTER FOUR

### 4.0 RESULTS AND DISCUSSION

#### 4.1 Particle Size Analysis Result

The particle size analysis results showed that coconut shell particles have grain fineness number (GFN) of 74.08. The sample was considered fine, because the GFN value of 100 is ranked the finest. Also, the sample was considered to have met the American Fraction Specification (AFS), since four sieve sizes have the bulk of the retained samples on four consecutive sieves in descending order, corresponding to 355, 180, 125, and 63 size fractions respectively. Morphology of the coconut shell by scan electron microscopy, SEM, with energy dispersive spectroscopy EDS are shown in Plate VII.

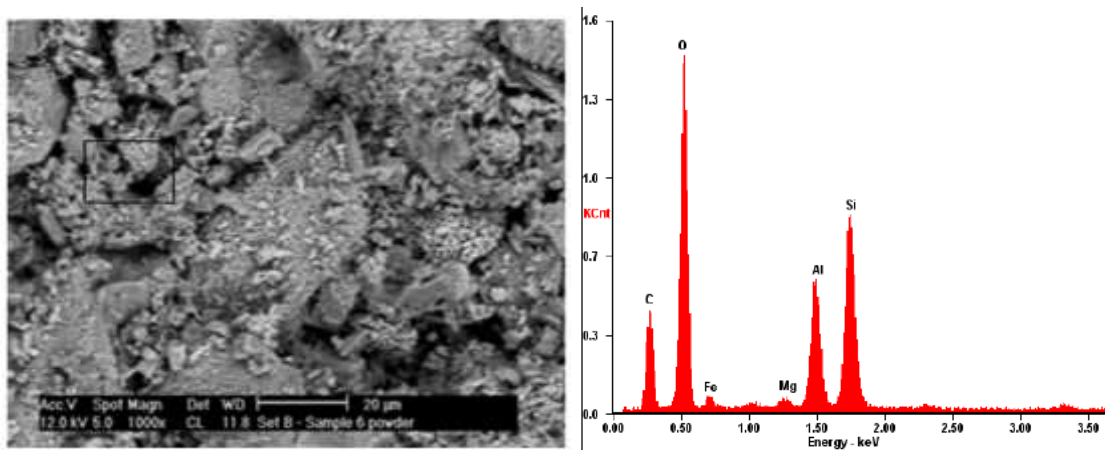


**Plate VII: Scan Electron Microscope Spectrum Figure 4.1 Energy Dispersive Spectrum (EDS) of Coconut Shell Ash (CSA) Particles**

The structure revealed that the size and shape of the particles varied, however, they were sorted into two main groups; spherical and fibrous. The spherical particles consist mainly of silicon Si, carbon C, and oxygen O as well as magnesium Mg, aluminium Al with small amounts of iron Fe, as shown in the EDS scan, Figure 4.1. The results were consistent with

that obtained by Bello et al, (2015). The SEM result showed that both SiO<sub>2</sub> and SiC have a fine structure.

The presence of hard elements like SiO<sub>2</sub>, Al<sub>2</sub>O<sub>3</sub> and FeO<sub>3</sub> in coconut shell ash, Table 4.1, suggested that, coconut shell can be used as particulate reinforcement in various metal matrices.

**Table 4.1 Composition of Coconut Shell Ash**

Element	Al <sub>2</sub> O <sub>3</sub>	CaO	FeO <sub>3</sub>	K <sub>2</sub> O	MgO	Na <sub>2</sub> O	SiO <sub>2</sub>	MnO	ZnO	Mullite
%	15.7	0.58	12.3	0.49	15.9	0.46	43.05	0.21	0.29	11.02

#### 4.2 Microstructural Analysis of Composites

The microstructure of the aluminium alloy, and that of the aluminium alloy with coconut shell ash were analysed, using scanning electron microscopy/energy dispersive spectrometry. The microstructure of the aluminium alloy is shown in Plate VIII. The structure reveals the eutectic phase containing Fe<sub>3</sub>Si, Al<sub>6</sub>Fe, in  $\alpha$ -aluminium matrix.

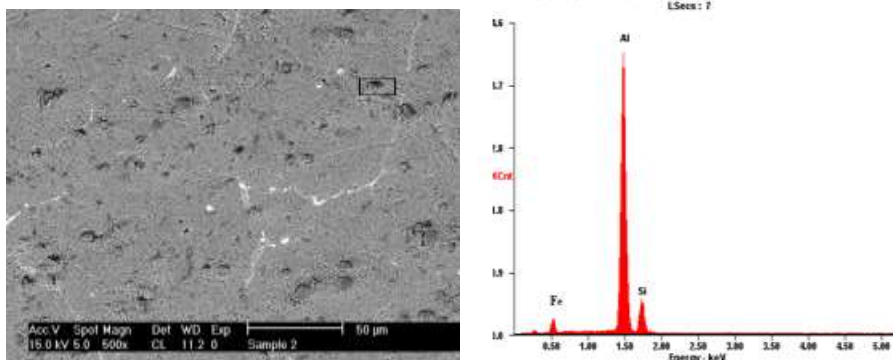


**Plate VIII: SEM of the Aluminium Alloy**

**Figure 4.2: EDS of Aluminium Alloy**

The microstructure of the composites can be seen in Plates IX-XIII. It was revealed that, there was a small discontinuities and reasonably a uniform distribution of coconut shell ash particles in the aluminium matrix. The ceramic phase was shown as the dark phase, while the metal phase was white (Plates IX-XIII).

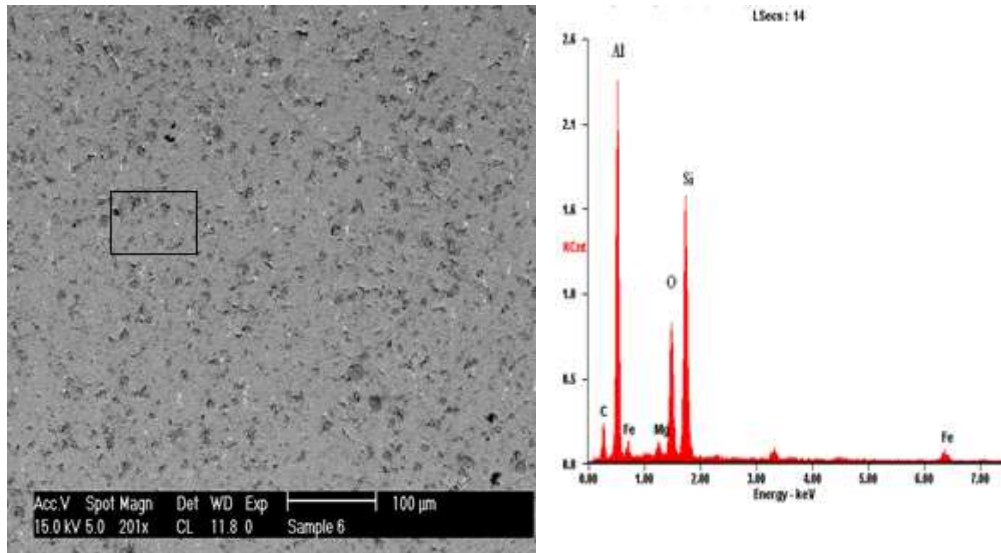
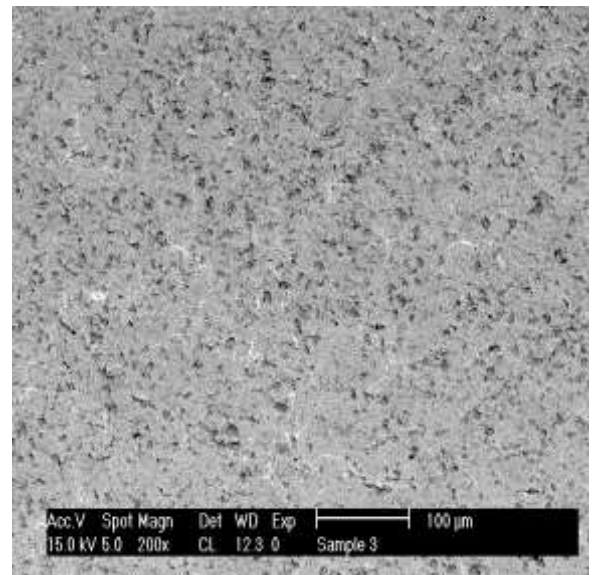
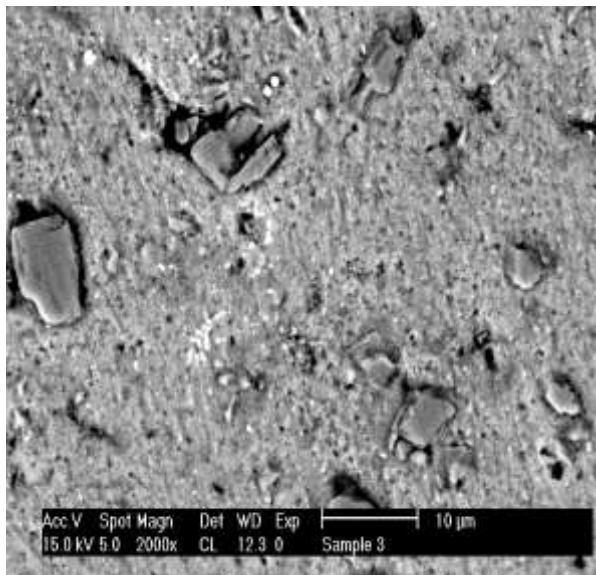


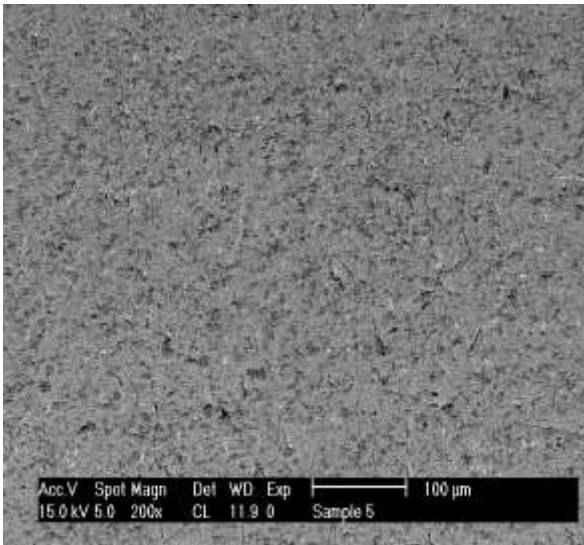
Figure 4.3: EDS of 3% by weight CSAp

**Plate IX: SEM/EDS of the Aluminium Alloy with 3% by weight CSAp**

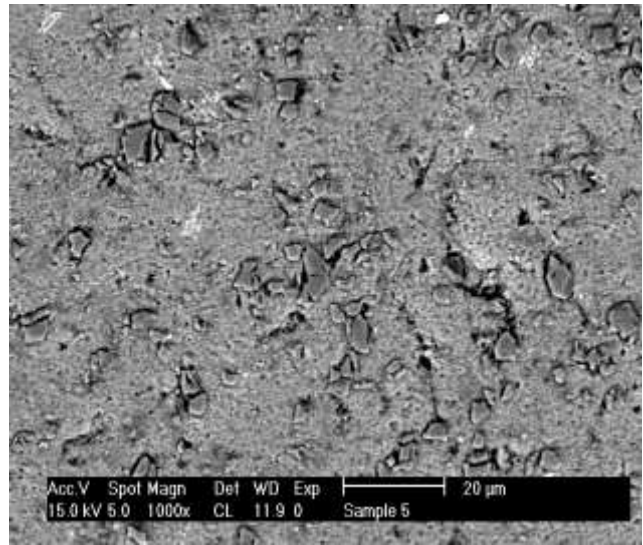


a) Higher magnification = 200 x      b) Lower magnification = 2000 x

**Plate X: SEM of the aluminium alloy with 6% by weight CSAp**

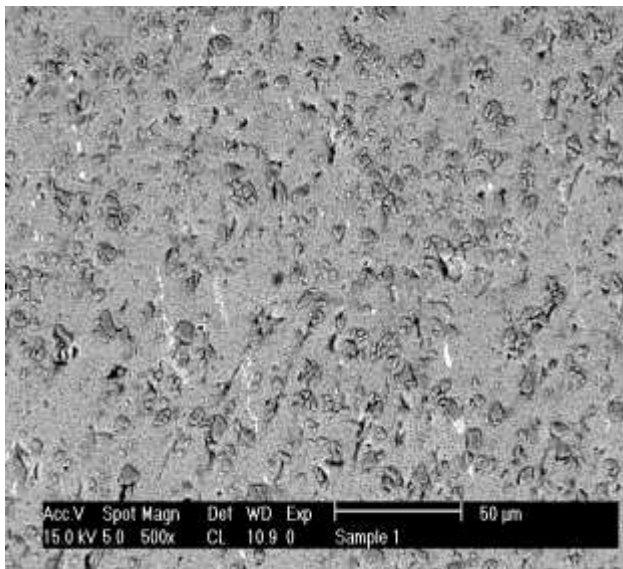


a) Lower magnification = 200 x

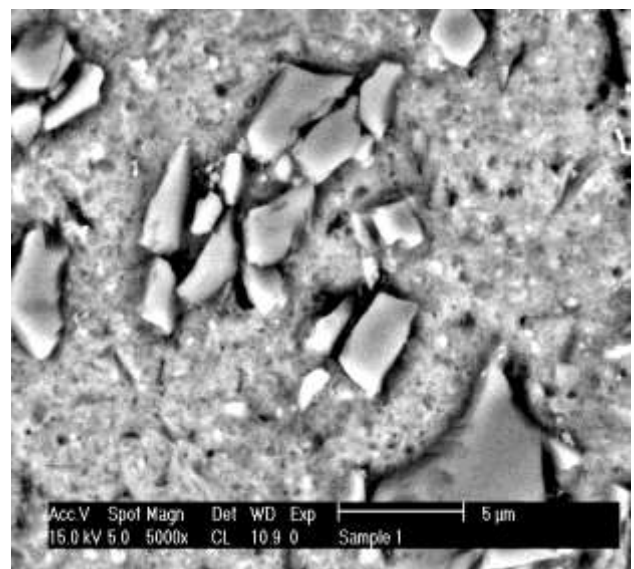


b) Higher magnification = 1000 x

**Plate XI: SEM of the aluminium alloy with 9% by weight CSap**

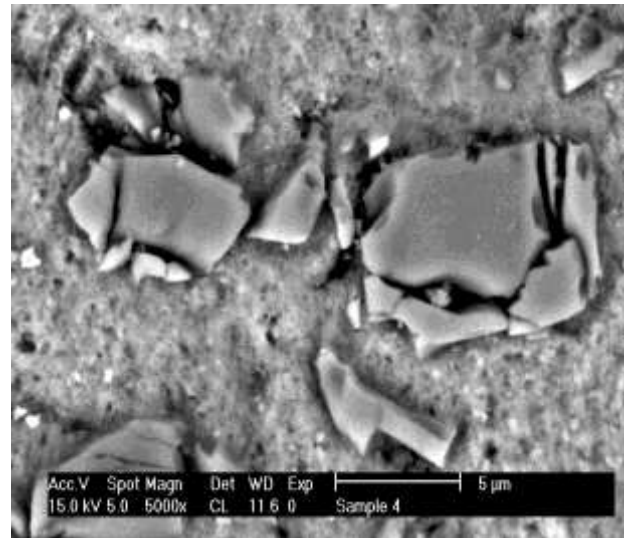
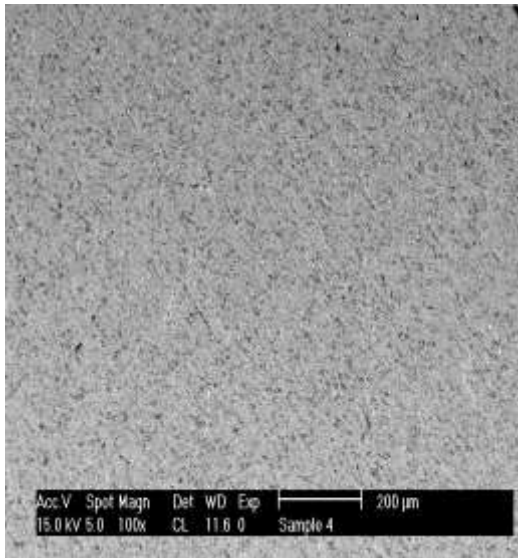


a) Lower magnification = 500x



b) Higher magnification = 5000 x

**Plate XII: SEM of the aluminium alloy with 12% by weight CSap**



a) Lower magnification = 100 x      b) Higher magnification = 5000 x

**Plate XIII: SEM of the aluminium alloy with 15% by weight CSAp**

These structures are in agreement with phases studied by other researchers, Chinthani, *et al.* (2015). The structure obtained in this work was made possible by activation of the coconut shell ash particles (CSAp) and proper selection of parameters for the casting process.

Electron transmission microscopy was used to analyse the interfaces between coconut shell ash particles and the matrix. The presence of the considerable amount of silicon and iron in the matrix alloy ensured the formation of the required bonds between the components of the composite and matrix examined. Interfaces between the particles and the matrix, were free from intermediary phases and any precipitates, had an adhesive effect on component bonding. Moreover, the samples were characterized by a high cohesion, without microcracks, and strength of bonding. The microstructure of the composite clearly showed a uniform distribution of coconut shell ash in the aluminium alloy matrix such as cast composites.

In the composites examined, no effects of unfavourable phenomena were observed, which usually formed in the structures of cast composites, such as sedimentation or flowing out

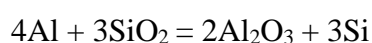


of the reinforcing phase, as well as the formation of particle agglomerates or gas blisters. This showed that there was a good interfacial bonding between coconut shell ash particles and the matrix. Good retention of coconut shell ash particles was clearly seen in the microstructures of the composites. Satisfactory interfacial bonding was obtained by heating of coconut shell ash particulates prior to dispersion and addition of magnesium in small quantities during stirring, which improved wettability of coconut shell ash particles.

Scanning electron micrographs of a typical coconut shell ash particle, which has retained the original shape of the coconut shell ash, are shown in Plate 4.1. However, these particles are quite fragile and some particles tend to break down during handling, thereby losing the hull like shape. In addition, aluminium dendrites, eutectic silicon and some small fragmented coconut shell ash particles can also be seen in the microstructure.

The chemical analysis was done by Energy Dispersive Spectrometer (EDS), using the sample prepared for Scanning Electron Microscope Scanning electron microscope (SEM). The analysis revealed the presence of silicon particles as a result of the reaction between the Coconut Shell Ash (CSA) particles and molten Al alloy. The peak value shows the presence of Al and its compound on the surface. The unreinforced alloy revealed the presence of  $\alpha$ -Al, Si and Fe as evident from the EDS spectra (Plate 4.2). From the EDS analysis of the composite (Plate 4.3), there were indications of some possible chemical reaction between aluminium melt and coconut shell ash particles, which led to the release of Si, Fe, O and C.

The diversified chemical composition of coconut shell ash particles and its high reactivity, can form compounds by chemical reactions between coconut shell ash particles and liquid aluminium during the synthesis of the composites. The reaction between CSAp-reinforcement containing silica and liquid aluminium, can lead to the formation of alumina and silicon in the following reaction:



The development of some primary silicon single crystals in the vicinity of coconut shell ash was seen in the Plate 4.3.

Electron transmission microscopy was used for the analysis of the interfaces between coconut shell ash particles and the matrix. The presence of considerable amounts of silicon and iron in the matrix alloy, ensured the formation of the required bonds between the components of the composite examined. Interfaces between the particles and matrix, are free from intermediary phases and any precipitates, had an adhesive effect on component bonding.

Moreover they were characterized by high cohesion (without micro-cracks) and strength of bonding. The microstructure of the composite clearly showed a uniform distribution of coconut shell ash in the aluminium alloy matrix. In the composites examined, no effects of unfavourable phenomena were observed, which frequently formed in the structures of cast composites, such as sedimentation or flowing out of the reinforcing phase, as well as the formation of particle agglomerates or gas blisters. This showed that there was good inter facial bonding between coconut shell ash particles and the matrix.

### 4.3 Thermal behaviour

The thermal stability of metal composite plays a crucial role in determining the limit of their working temperatures and the environmental conditions for their uses, which are related to the thermal decomposition temperature and decomposition rate. Figures 4.4 and 4.5 show plates of DTA/TGA decomposition data of Al-Si-Fe alloy and its composite at 15%CSAp.

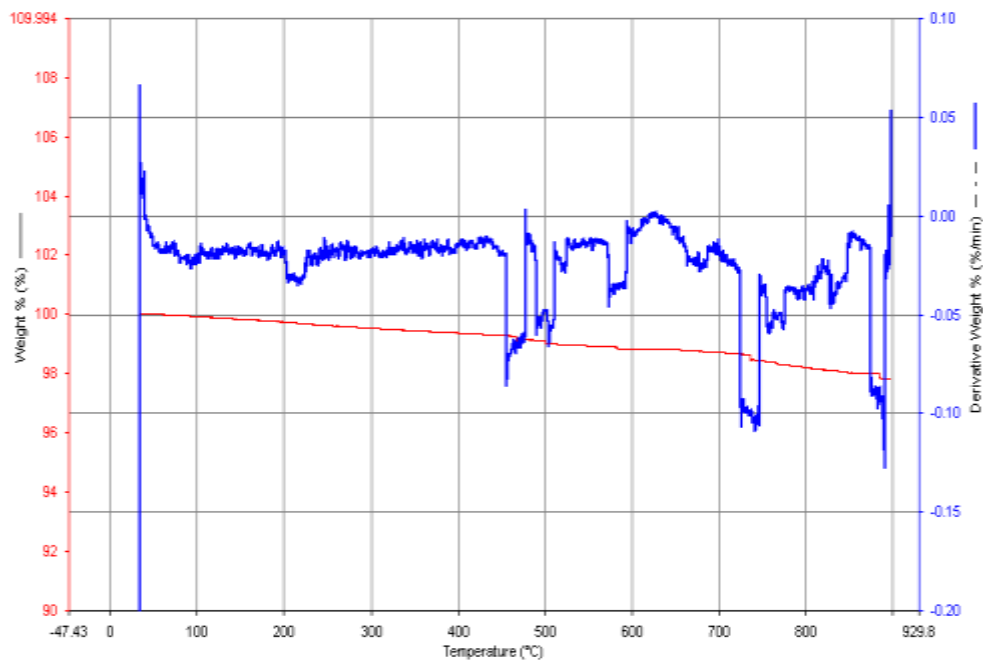


**Figure 4.4: DTA/TGA of Al-Si-Fe Alloy**

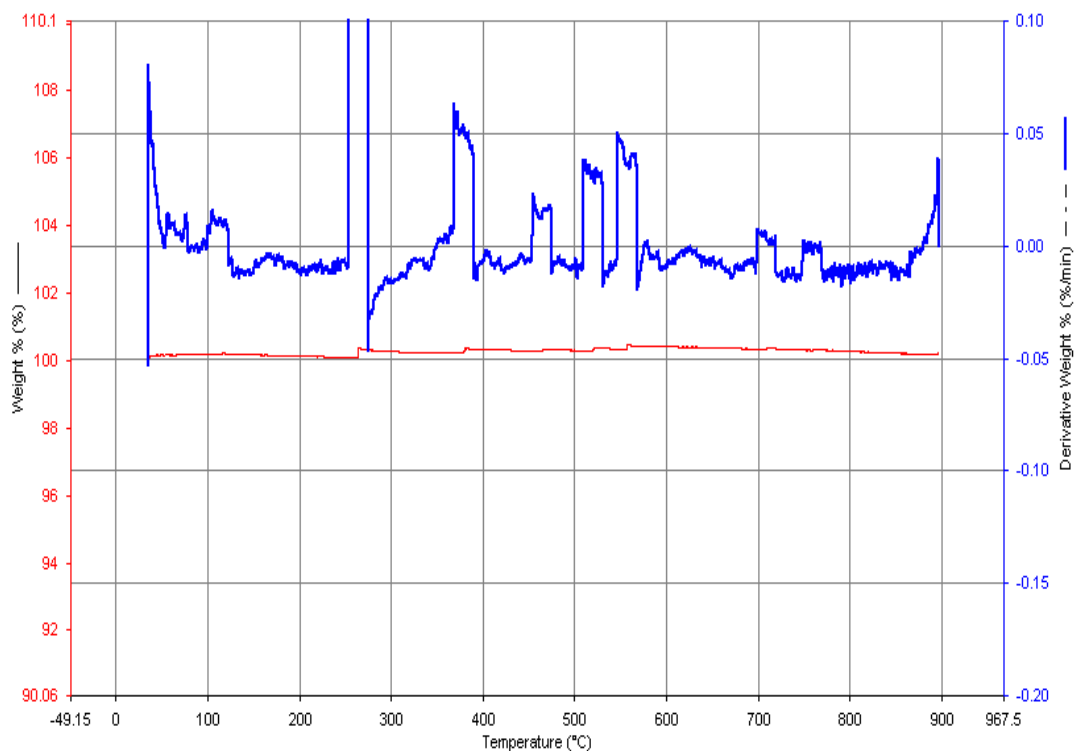


**Figure 4.5: DTA and TGA of Al-Si-Fe Alloy/15% by weight CSAP**

The patterns of TGA curves for the composite are similar, implying that the thermal decomposition of Al-Si-Fe/CSAp composite may mostly stem from Al-Si-Fe alloy. From the curves, the temperature of maximal decomposition and destruction, fall within 700-800. The pronounced single endothermic effects observed in the DTA curves correspond to the oxidative degradation process and the release of volatile matters. From the DTA curves, the temperature of maximal decomposition and destruction of the Al-Si-Fe alloy/CSAp composite fall between 700 to 800 (Figures 4.4 and 4.5)

The total burning and degradation of the residual Al-Si-Fe took place at the temperature interval of 600 to 700. In the last temperature interval the mass loss was minimal; this last step was due to the degradation of the CSAP material in the composite. The result indicated that the Al-Si-Fe alloy/CSAp composite biomass show less percentage of decomposition. At temperature above 700<sup>0</sup>C, the residual weight stabilized and agreed with the silica and carbon content earlier reported in literature.

As shown in Figures 4.1 and 4.2, incorporation of the CSAp into Al-Si-Fe alloy matrix increased the thermal decomposition temperatures and residual yields of Al-Si-Fe alloy/CSAp composite. This result indicated that the presence of CSAp led to the stabilization of Al-Si-Fe alloy, and resulted in the enhancement of the thermal stability of the composite. In the composite, the CSAp acted as barriers to prevent the transport of the volatile decomposed products out of the composite during thermal decomposition.

#### **4.4 Fourier Transform Infrared (FTIR) analysis of the coconut shell ash particles**

Eleven main peaks were detected in the FTIR analysis of the coconut shell ash as visible in Figure 4.6. The result showed that the presence of quartz in the original ash gave rise in the IR spectrum to a series of bands located at 1107 and 70.03  $\text{cm}^{-1}$ . The presence of mullite, in turn, is responsible for a series of bands at around 2113  $\text{cm}^{-1}$ . The presence of carbon in a series of bands at around 1908.4-1997.9  $\text{cm}^{-1}$ . Quartz, mullite and the vitreous phase of the ash overlap in the area between 1030.2  $\text{cm}^{-1}$  and 1107.7  $\text{cm}^{-1}$ . Hence, quartz, mullite, carbon and vitreous phases were confirmed to be present. However, the peaks in treated and untreated cases do not show any variations.

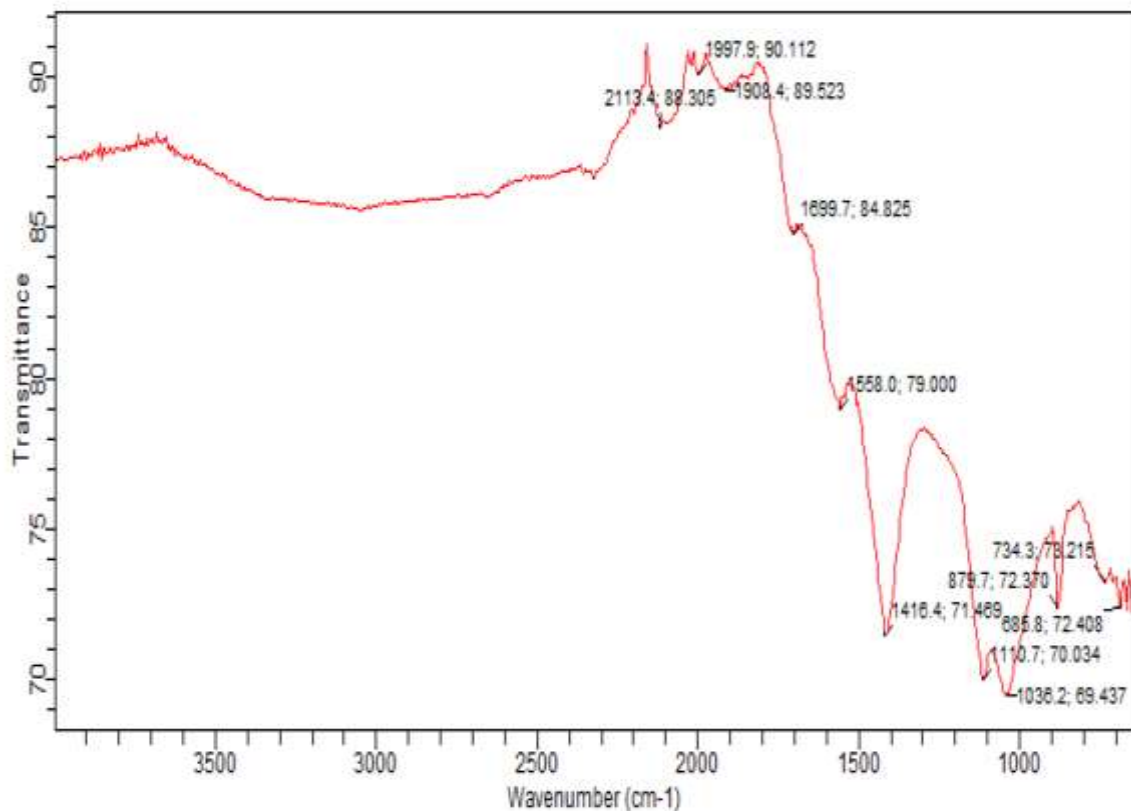


**Figure 4.6 FTIR Spectrum of the Coconut Shell Ash**

#### 4.5 Composite Hardness Values

Hardness of the developed composites increased with increase in percentage of coconut shell ash particle additions as shown on Table 4.2 and Figure A1 (in Appendix). It is noteworthy that the hard value of coconut shell is 78.6HRB and the presence of the hard ceramic phase in the ductile matrix has resulted in the increase in hardness of the composite (Table 4.1). For example, the hardness values increased from 63.50HRB at 0wt% to 78.60HRB at 15wt% coconut shell ash particles. This hardness of the coconut shell ash particles was obtained from the SiC, Al<sub>2</sub>O<sub>3</sub>, FeO<sub>3</sub> and SiO<sub>2</sub>, in the chemical makeup of the particles (Table 4.1). The presence of coconut shell ash particles in the alloy also increased the dislocation density at the particle-matrix interfaces. This was as a result of difference in the coefficient of thermal expansion (CTE) between the hard and brittle reinforced particles, and soft and ductile metal

matrix which resulted to elastic and plastic incompatibility between the matrix and the reinforcement (Issac *et al.*, 2016).

**Table 4.2: Hardness Test Results of the Composites**

Wt% CSAp	1 <sup>st</sup> reading	2 <sup>nd</sup> reading	3 <sup>rd</sup> reading	Average(BHN)
0	63.00	64.00	63.50	63.50
3	67.00	68.90	69.00	68.30
6	69.50	68.90	70.50	69.13
9	70.00	69.50	75.20	70.00
12	76.00	75.50	75.20	75.40
15	78.50	78.60	78.70	78.60

#### 4.6 Tensile and Yield Strength Test Values

The tensile and the yield strength were carried out on the piston which was produced by double stir casting, the values obtained are shown in Table 4.3 and Figure A2 (in Appendix).

**Table 4.3: Tensile and Yield Strength at 0.2% Upset**

Wt% CSAp	TS (N/mm <sup>2</sup> )	YS (N/mm <sup>2</sup> )
0	159.84	112.65
3	160.23	112.85
6	186.05	130.57
9	200.77	145.65
12	196.77	196.77
15	196.05	196.05

The results indicated that the yield and tensile strengths increased to 28.38 and 24.86% at 12%CSAp respectively. With increasing volume fraction, more loads were transferred to the reinforcement which also resulted to a higher tensile strength. This behaviour is in agreement with Yuan, *et al.* (2015).

Plates XIV and XV show the typical fractographs of the failed tensile samples. The composite samples display a mixed fracture mechanism on the fracture surface, brittle fracture of the reinforcement particles and ductile tearing of the aluminium alloy matrix.

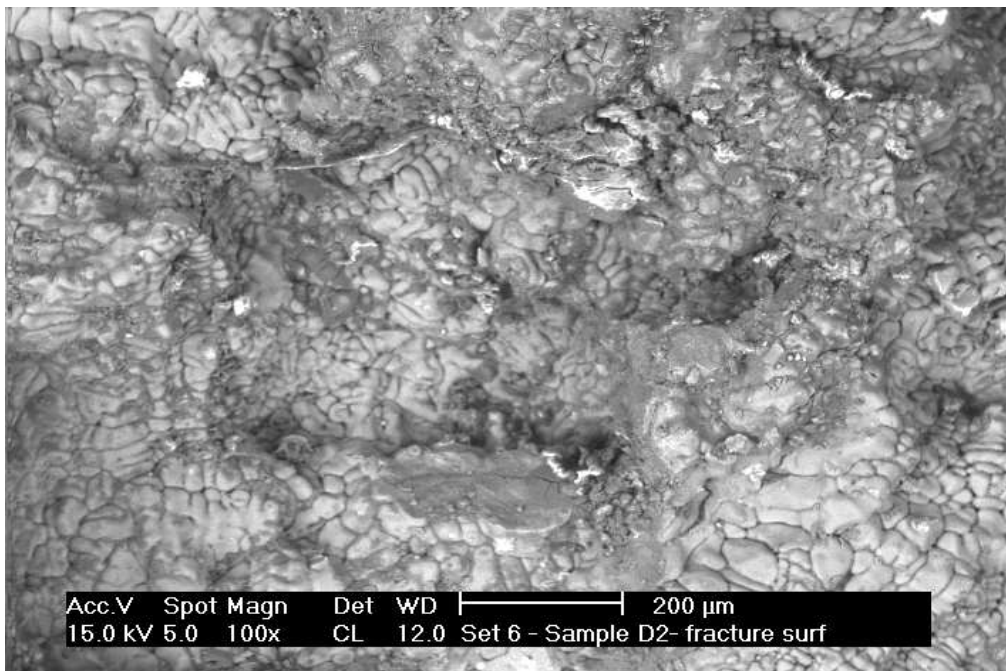


**Plate XIV: SEM Fractographs of the aluminium alloy**



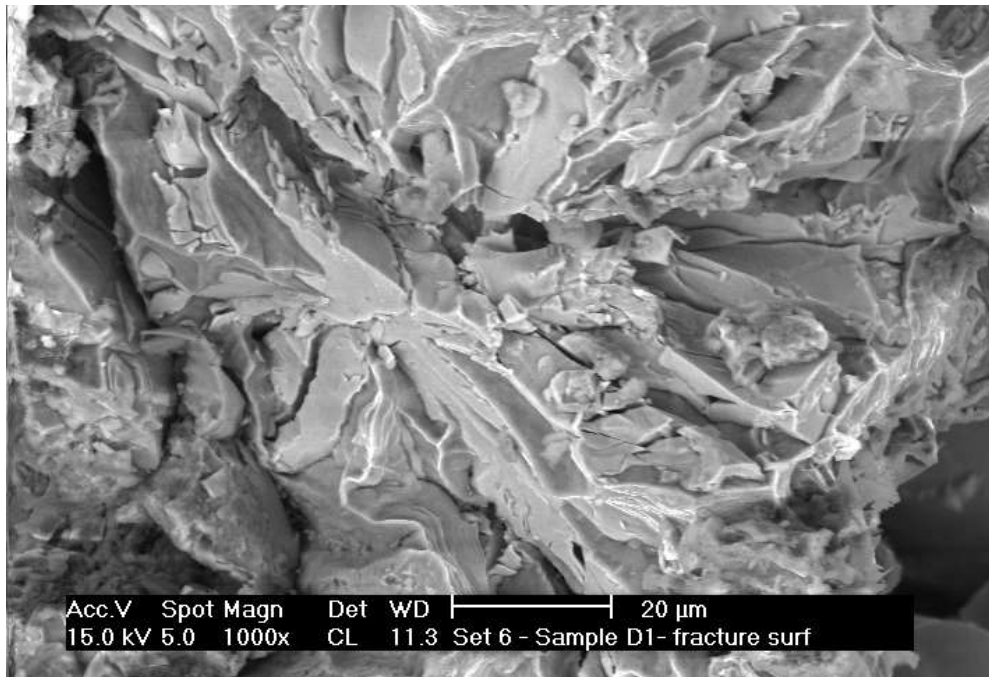


**Plate XV: SEM Fractographs of the aluminium alloy reinforced with 15wt% CSAp**

The primary difference between the fractured surfaces of the composites is the relative area fraction of the matrix to fractured particles. Another difference is the proportion of voids presented on the fractured surface. From Plates XIV and XV, it can be concluded that the dominant fracture mode of samples are particle cracking and matrix ductile tearing. Particle-matrix interfacial de-bonding cannot be found by fracture surface examination, which confirms the strong interfacial bonding between the CSAp and the aluminium alloy matrix (Itskos *et al.*, 2011).

#### **4.7 Density Values of the composites**

The results of the density measurements on alloy and reinforced materials, as shown in Table 4.4 and Figure A3 (in Appendix), revealed that an increase in the percentage of coconut shell ash in MMC, decreased the material density. This is due to the fact that the coconut shell ash particles are less dense compared to aluminium alloy. The density of the reinforced coconut shell particle composites decreased from 2.8g/cm<sup>3</sup> at 0wt% of CSAp addition to 2.66g/cm<sup>3</sup> at 15wt% of CSAp addition. This revealed that composites with light weight can be made with this ash. The result is in agreement with earlier work of Prasad and Krishna (2010).

**Table 4.4: Density of the Composites**

Wt%CSAp	Mass (g)	Volume (cm <sup>3</sup> )	Density (g/cm <sup>3</sup> )
0	5.50	1.93	2.85
3	6.00	2.12	2.83
6	5.00	1.89	2.75
9	5.58	2.07	2.70
12	6.20	2.68	2.68
15	5.89	2.66	2.66

#### **4.8 Wear Behaviour and Coefficient of Friction**

The SEM microstructure of the worn surfaces are shown in Plates XVI and XVII.

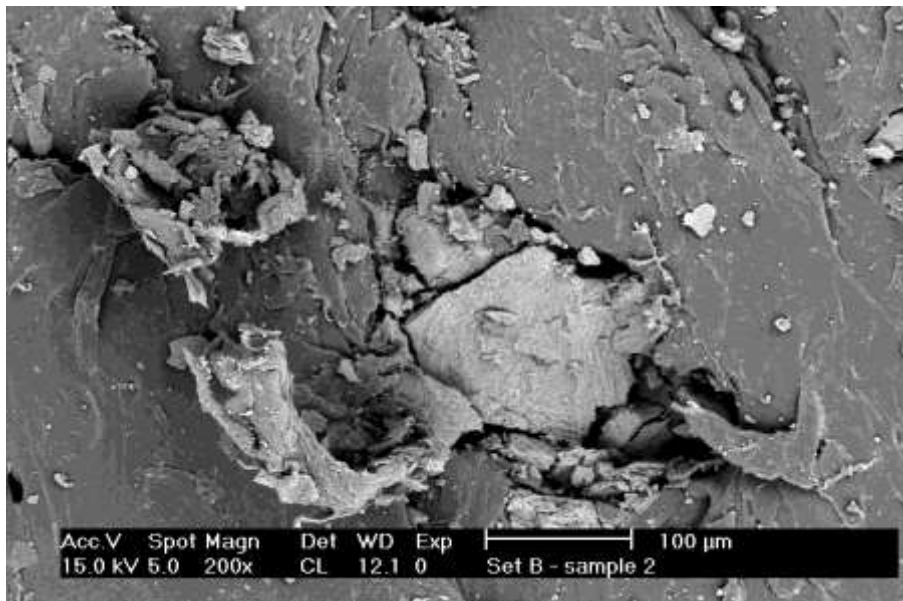


**Plate XVI: SEM of the worn surface of the aluminium alloy at 50N, 2.0m/s and 400mm. These represent wear test conducted by varying applied load from 10 to 50N at a constant speed of 2.0m/s and a sliding distance of 400mm**

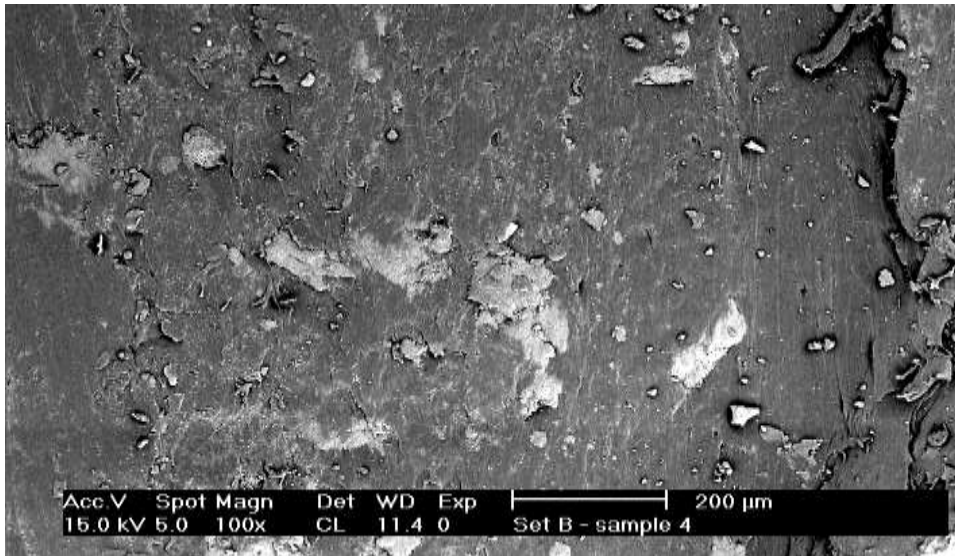


**Plate XVII: SEM of the worn surface of the aluminium alloy with 9% by weight CSAp at 50N, 2.0m/s and 400mm of varied applied load.**

From Plates 4.10 and 4.11, it can be seen that the aluminium alloy with no CSAp reinforcement formed a good thin and uniform transfer film (Plate XVI). In the case of aluminium alloy with CSAp reinforcement (Plate XVII), there appeared to be some disruption of the transfer film for CSAp which affected the wear rate performance. The worn surface of the materials can be described as classical ratcheting wear, as defined by Monikandan, *et al*, (2016).

The transition in wear rate observed for many MMCs is faster and is believed to be the result of voiding/cracking between the reinforcement and the matrix, both of which led to fragmentation and delimitation of the surface (Monikandan, *et al*, 2016). Plate XVII revealed particle cutting and void formations due to chips of the matrix. There is also evidence of Al-Si-Fe alloy removal, and deep furrows in the structure.

The propagation of cracks along transverse, as well as longitudinal directions is well visualized. Furthermore, crushed and fragmented particles were noticed in Plate XVI. The worn surfaces in some places revealed patches from where the material was removed from

the surface of the material. The parallel grooves suggested abrasive wear as characterized by the penetration of the hard coconut shell ash particles into a softer surface, which is an important contributor to the wear behaviour of Al-Si-Fe/CSAp composites. It is possible that the scored grooves might have been formed due to the action of the wear-hardened deposits on the disc track. Similar observations were made by Monikandan, *et al*, (2016).

The results of the wear rate and coefficient of friction are shown in Table 4.5 and 4.6 and Figure A4 and A5 (in Appendix) respectively.

**Table 4.5: Wear Rate of the Composites (mm<sup>3</sup>/Nm)**

Wt% CSAp	10N	20N	30N	40N	50N
0	3.4	3.5	4.8	5.8	7.3
3	3.4	3.4	4.0	5.0	6.8
6	2.8	3.0	4.0	4.5	6.0
9	2.2	2.56	3.5	4.0	5.4
12	1.8	2.0	3.0	3.2	5.0
15	1.2	2.8	2.8	3.0	4.8

From Figure A4 (in Appendix), it was observed that the wear rate increased with decrease in the weight percentage of coconut shell ash particles. Also, increase in applied load resulted to increased wear rate of the samples for all composites of coconut shell ash. At higher applied loads, the samples got well spread with less coconut shell particles getting exposed, and breakages of CSAp taking place. This is attributed to fragmentation of the CSAp and its detachment from the test material, due to the non-availability of a medium to hold them. The

beneficial effects of the reinforcement on the wear resistance of the Al-Si-Fe alloy composites was observed to be the best at low loads, and reduced with increase in applied load. With higher loads, contact temperatures became higher, and plastic deformation occurred with consequences of higher wear. Also, when applied loads were increased, seizure was accompanied by sudden increase in wear rate, and heavy noise with vibration were also noticed. This type of seizure has been referred to as galling seizure (Hubert *et al.*, 2014). The wear mechanism reported was oxidation at lower loads, and adhesion and delimitation at higher loads (Yuan *et al.*, 2015).

Friction and wear will increase due to the critical surface energy of the MMCs. Furthermore, this explained the frictional heat raised, raising the temperature of the friction surfaces. It has been established that the wear process involves fracture, tri-bio-chemical effects and plastic flow. Transitions between regions dominated by each of these, give rise to changes in wear rate with load. Table 4.6 shows the values of coefficient of friction of the aluminium matrix composite at different loads and proportions of the coconut shell ash reinforcement.

**Table 4.6: Coefficient of friction of the composites at different loads and Wt%CSAp**

Wt%CSAp	10N	20N	30N	40N	50N
0	0.2	0.25	0.45	0.55	0.58
3	0.23	0.35	0.50	0.65	0.67
6	0.23	0.39	0.54	0.65	0.68
9	0.30	0.395	0.58	0.67	0.73
12	0.33	0.40	0.60	0.69	0.78
15	0.38	0.43	0.60	0.72	0.80

The frictional forces rise in the initial period and then fluctuate around the mean during dry sliding. The mean was determined from the individual values of coefficients of friction, excluding the initial rising part. It was observed that the mean coefficient of friction increased

with increasing load for the Al-Si-Fe alloy, and the composites containing CSAp as shown in Table 4.6 (Figure A5) at higher loads, the frictional force increased with greater dissipation of energy, leading to higher temperature at contact, which resulted to a higher coefficient of friction with increasing load.

The MMC exhibited high wear resistance under different applied loads. This could be attributed to the presence of CSAp on the counter surface, which acted as a transfer layer and effective barrier to prevent large scale fragmentation of the Al-Si-Fe matrix. The wear resistance of the composite is improved by preventing direct contact that induces surface deformation. The addition of hard ceramic particles improved resistance to seizure. Coconut shell particulate allowed considerable thermal soften effects without having adverse effects on wear behaviour. The reinforcement also caused higher hardness at lower coefficient of thermal expansion of the Al-Si-Fe alloy matrix, as demonstrated in Figure A4 (in Appendix). The presence of the ceramic particles provided higher thermal stability, increased abrasion and sliding wear (Bhagat, 2011).

The wear rate increased with increasing applied load, while it decreased with increasing volume fraction of the CSAp material. This may be due to the reason that, addition of ceramic content resulted in a pronounced drop in ductility, accompanied by an increase in hardness, which may further increase the wear resistance of the composites. At any load, wear rate decreased with increase addition of CSAp, and improved the load bearing properties of Al-Si-Fe alloy matrix during sliding. The addition of CSAp restricted the flow deformation of the matrix with respect to load. This is because, whenever applied load increased, the friction at the surface of the material and rotating the disc obviously increased.

#### 4.9 Corrosion behaviour

Table 4.7 (Figure A6) show the variation of corrosion rate with time for Al-Si-Fe alloy and its composites in neutral 3.5% by weight of salt solution.

**Table 4.7: Average values for weight loss (mg) of the composite immersed in 3.5% by weight NaCl solution**

Wt % CSAp	1Day	3Days	6Days	9Days	12Days	15Days
0 wt% CASP	2.8816	1.0673	1.7464	0.0534	0.0534	0.0427
3 wt% CASP	3.2244	2.1496	1.3435	1.2181	0.0914	0.086
6 wt% CASP	4.9773	3.3182	1.659	1.4379	1.2443	1.1061
9 wt% CASP	5.6512	3.9429	2.2531	1.8776	1.549	1.13293
12 wt% CASP	5.6713	4.5398	2.27	2.0807	1.8443	1.4981
15 wt% CASP	5.6714	4.5739	2.5728	2.2107	2.001	1.7152

The corrosion rate of the materials increased slightly as CSAp content increased, with the unreinforced alloy and Al-Si-Fe/15% by weight CSAp losing the least and greatest weights, respectively. It can be seen that the matrix alloy (Al-Si-Fe) and its composites showed similar corrosion behaviour. The corrosion rates of all the tested materials decreased rapidly during the first three days of exposure to the electrolyte but, with further exposure time, the decrease was very gradual.

Passivation of the matrix alloy is believed to be responsible for the monotonic decrease in corrosion rate, with increasing exposure time observed in these materials. It was also seen that Al-Si-Fe/15% by weight CSAp showed the highest rate of corrosion. It was observed that the corrosion of the composites was accompanied by the loosening of CSAp particles. It is believed that the corrosion of the CSAp-matrix interface caused the loosening of CSA particles, which were finally dislodged from the specimen during the post-immersion cleaning process. Similar observations were made by Orhorhoro *et al.* (2017), who reported that fly ash particles acted as pit initiation sites in fly ash/Al-Si alloy composites, and that there was a

build-up of corroded fly ash particle debris in corrosion pits. The loss of such particles during post- immersion cleaning, contributed to the high weight loss recorded for the composites in the present study.

Engineering materials used for construction and other applications for example automotive pistons, experience different forms of interactions with different environments. The service life of such an engineering component such as the automotive piston depends on its ability to resist degradation.

Studying the physical properties such as density and porosity of the developed composite therefore, is significant because strength, stiffness as well as its low density are properties that are well suited for weight-sensitive automotive and other industrial components and parts.

Since corrosion decreases the load-bearing capacity of parts, resulting in catastrophic failures, studying the corrosion properties of the MMC can limit the application of such components in corrosion environments, especially in the presence of stresses (Karthikaiselvi and Subhashini, 2014).

#### **4.10 Performance Evaluation Results**

The time taken to consume 100ml of fuel using conventional standard piston was 16.5 minutes against 18 minutes when aluminium matrix composite (AMCs) was used. The time for the engine to consume 200ml fuel was 20 minutes for the conventional piston against 22 minutes. Table 4.8 and 4.9 show the fuel consumption rate, engine speed, ambient temperature and periods at which experiment were conducted.



**TABLE 4.8: PERFORMANCE TEST (STANDARD PISTON)**

S/No	Description	Time	Duration	Ambient Temp. °C	Fuel Consumption (lit/min)	Average Voltage	% Fuel Consumption /min	Average Idle Speed (rpm)	
1.	100 ml (0.1 litre) of petrol	10.15am am	10.31 am	16.5	31	0.1/16.5 = 0.006	13.8	0.6	800
2.	200ml (0.2 litre) of petrol	10.30 am	10.45 am	20	31	0.2/20 = 0.010	13.8	1	900
3.	250ml (0.25 litre) of petrol	10.55 am	11.20 am	24	31.5	0.25/24 = 0.010	13.8	1	1000
4.	300ml (0.3 litre) of petrol	10.45 am	11.15 am	30	32	0.3/30 = 0.010	13.8	1	1100

3.6

**TABLE 4.9: PERFORMANCE TEST (MMC PISTON)**

S/ No	Description	Time	Duration n	Ambient Temp. °C	Fuel Consumption (lit/min)	Average Voltage	% Fuel Consum n	Average Idle Speed (rpm)
1.	100 ml (0.1 litre) of petrol	Initial 10.20am Final 10.38am	18	31	0.1/18 = 0.006	13.8	0.5	800
2.	200ml (0.2 litre) of petrol	10.55 am 11.17am	22	31	0.2/22 = 0.010	13.8	0.9	900
3.	250ml (0.25 litre) of petrol	11.05am 11.21am	26	31.5	0.25/26 = 0.010	13.8	0.96	1000
4.	300ml (0.3 litre) of petrol	11.25 am 11.58am	33	32	0.3/33 = 0.010	13.8	0.9	1100
5.								

3.26

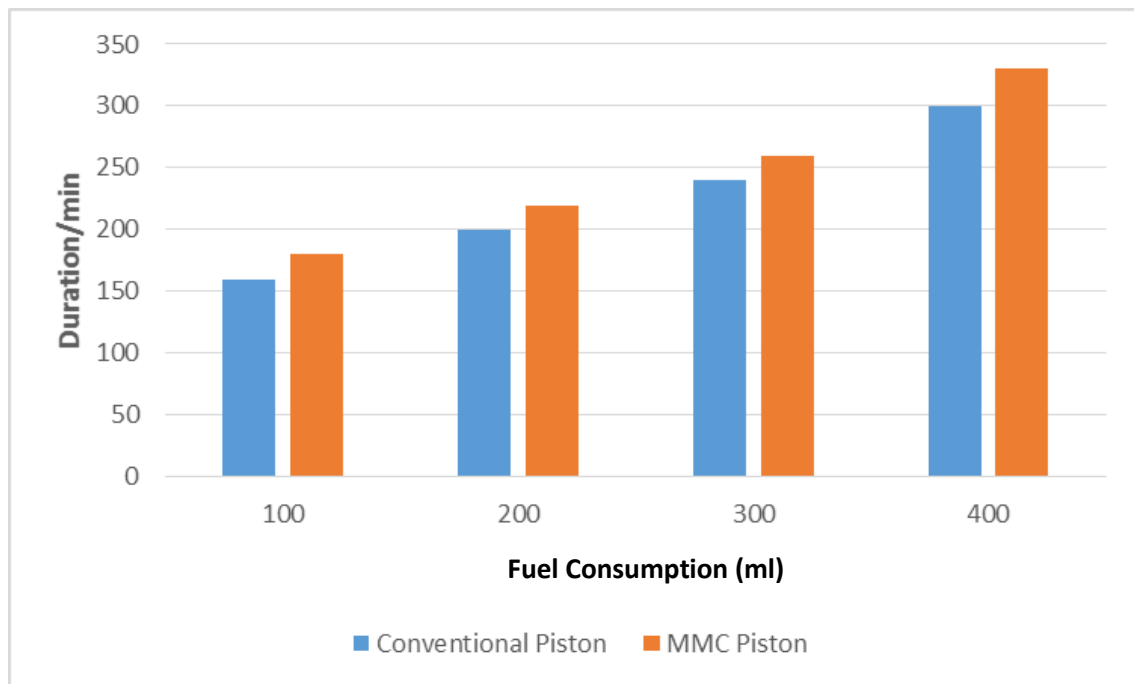


**Figure 4.7: Performance Evaluation of Conventional and MMC Piston**

From the performance test analysis (Figure 4.7), it was observed that the duration of fuel consumption for both types of pistons were similar for the regular pistons, the rate varied from 0.36KWh to 0.8KWh, while that of the developed pistons, the rate varied from 0.33KWh to 0.73KWh. The developed pistons consumed less fuel as the duration of running of the engine increased.

Also, from the brake force analysis (Figure 4.8), it was observed that the developed composite had lower brake force than the regular pistons. But for both pistons, as the speed increased, the brake horse power also increased. These results are in line with that of Firdaus *et al.* (2020).

If the regular piston is replaced with a composite piston, it will give improved performance. From results of forces acting on the piston, and from comparison of steel and MMCs pistons made by Keneth *et al.* (2014), it was clear that stress induced in composite piston was lower than that of the regular piston. Hence, the replacement of piston material with MMC gave improved strength, minimize weight and reduce induced stresses in the structure. Fuel saving of 0.0034 litres/min was achieved with composite pistons during performance tests, thereby increasing the strength to weight ratio.

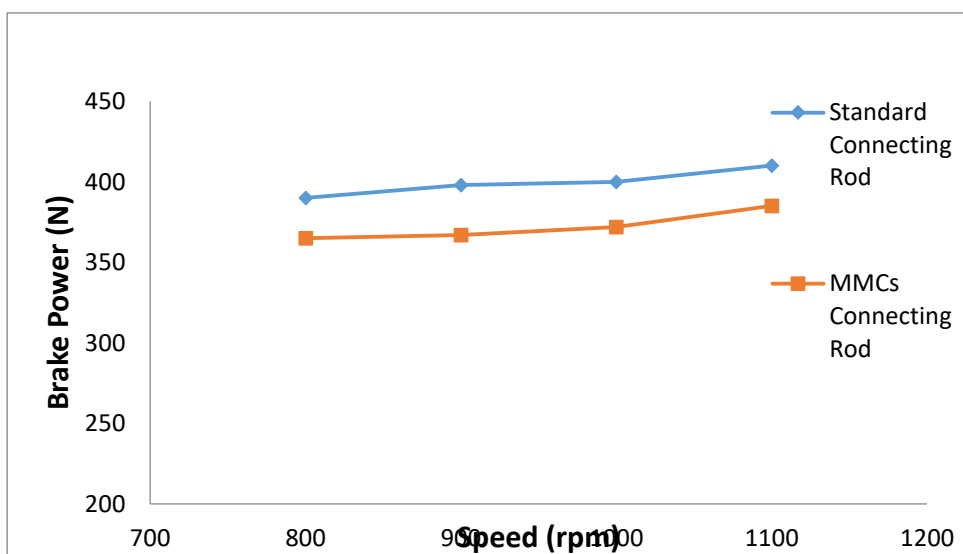


**Figure 4.8: Variation of Brake force with Engine speed ratio**

The performance tests showed that the engine fuel consumption when using the MMC pistons was lower than that of regular pistons, resulting in a 0.34% savings in fuel consumption, leading to lower running costs. From the brake force analysis, it was observed that the developed composite pistons had lower brake force than the regular pistons.

#### 4.11 Validation of Results

The properties of aluminium alloy reinforced with coconut shell ash, with results obtained by (Tadala *et al.*, 2016), (Sivaramakrishnan, *et al.*, 2019) and (Vinod and Mittal, 2013) are presented in Table 4.10.

**Table 4.10: Properties of Produced MMC Piston with Previous Research**

S/No	Authors	Ultimate tensile strength	Yield strength	Density	Thermal Conductivity
1	(Tadala <i>et al.</i> , 2016)	145	193.38	2.71	180
2	(Sivaramakrishnan, <i>et al.</i> , 2019)	199	196	2.78	120
3	(Vinod and Mittal, 2013)	169	195	2.78	121
4	Present work	200.77	196.77	2.66	172

Comparison of these results are shown in Figure 4.12. The variance in the properties were as a result of the materials used for reinforcing aluminium alloy.

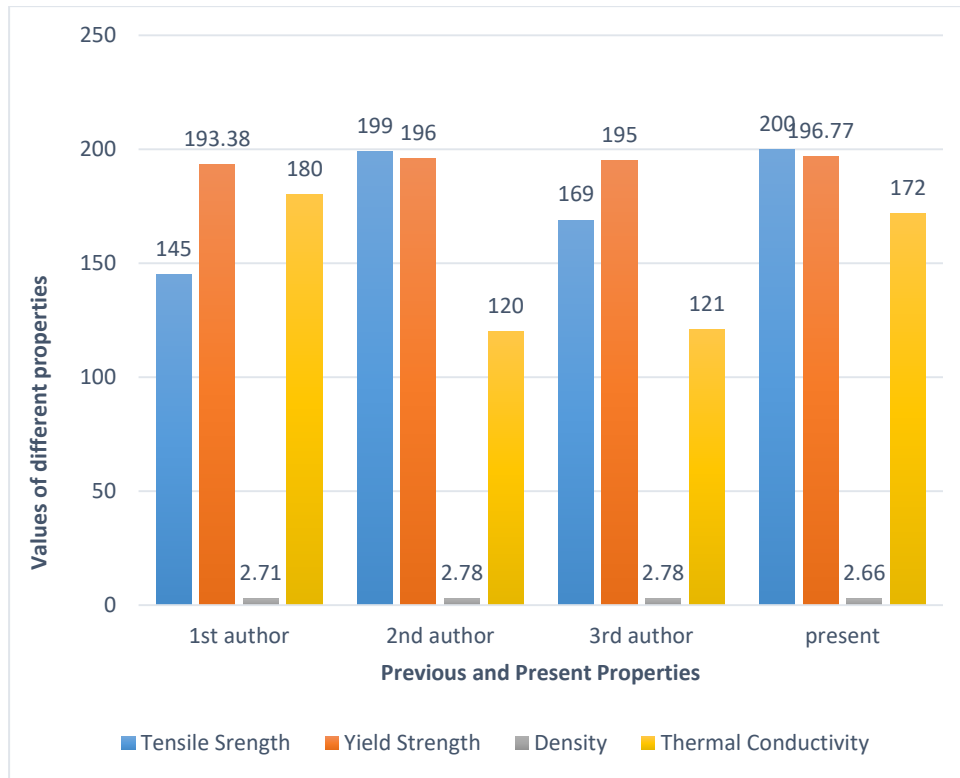


**Figure 4.9: Comparison of Properties of Produced MMC Piston with Previous Research**

Tadala *et al.* (2016) used Al-GHS 1300, Al-SiC-Graphite and Al 6061 pure aluminium to form the composite, Sivaramakrishnan, *et al.* (2019) used Al-alloy A-2618 and Al-GHS 1300 coated with Zirconium while Vinod *et al.* (2013) did not reinforce the aluminium alloy and the material used was Al 2024-T4, 2024-T35. The tensile and yield strength of the present work were higher than the previous work, while the density was lower. The thermal conductivity, 172 W/m-K, is considerably stable for piston operation, because the standard piston has thermal conductivity of 174.15W/m-K (Venkata *et al.*, 2013).

The hardness test conducted is compared with the other results are as shown in Table 4.11

**Table 4.11: Hardness Test Comparison**

<b>Aluminium (%)</b>	<b>Fly Ash (%)</b>	<b>Hardness (BRN)</b>
95	5	53
90	10	56.2
85	15	58.9
80	20	60.15

Source: Barekar, *et al*, (2008)

It was observed from the results of Table 4.10, at 20wt% fly ash, the hardness was 60.15 BRN. In the present research, at 15wt%, 78.6BRN was achieved, which is an improvement on the previous work. The variance was as a result of the material used for reinforcement of the aluminium alloy.

## CHAPTER FIVE

### 5.0 CONCLUSION AND RECOMMENDATIONS

#### 5.1 Conclusion

Aluminium matrix composites (AMC) reinforced with different volume fractions of coconut shell ash particles were fabricated by the double stir-casting method. The microstructures and properties of the composites were characterized and the following conclusions were drawn:

- i. Coconut shell ash particles were successfully incorporated in Al-Si-Fe alloy by using the stir casting technique.

The microstructure analysis of the composites revealed the uniform distribution of the coconut shell ash particles in the matrix. The increase in reinforcement volume fraction resulted in decrease of matrix grain size in the composites.

- ii. The addition of coconut shell ash particles reinforcement to Al-Si-Fe alloy increased the tensile strength and the hardness value of composites, but slightly reduced the impact energy.
- iii. The increase in strength and hardness was as a result of the increases in the amount of the hard coconut shell ash phase in the ductile metal phase, which led to increase in dislocation density at the matrix-particle inter phase.
- iv. Fracture mode of composites is particle cracking and matrix ductile tearing.
- v. It was observed that, as the applied load increased, the wear rate also increased. This is because, whenever applied load increases, the friction at the contact surface of the material and rotating disc obviously increased.
- vi. The coefficient of friction increased with increasing load for the Al-Si-Fe composite and the composites containing CSAp.



- vii. The Al-Si-Fe alloy/CSAp composite, the CSA particles act as physical barriers which prevented the transport of volatile decomposed products out of the composite during thermal decomposition.
- viii. The corrosion rate of the composites increased slightly with increasing CSAp, but decreased with exposure time.
- ix. Incorporation of coconut shell ash particles in aluminium matrix can lead to the production of low cost aluminium composites, with improved hardness and strength. These composites can find applications in automotive components where lightweight materials are required, with good stiffness and strength that can lead to piston production and testing.
- x. For optimum service performance of this alloy, coconut shell addition should be between 6-9% by weight, and not exceed 9% in order to develop better enhance properties. These composites can be used in the production of automotive piston since aluminium composites used in production of these components have similar properties as those of Al-Si-Fe/CSAp composites.
- xi. The produced MMC piston was tested in a 12 valve Toyota automobile engine. The result obtained showed a 3.6% fuel consumption/minute as against 3.26% fuel consumption/min are of the same quantity of fuel in the engine of a regular piston, and the MMC piston respectively, which translated to savings in running costs.
- xii. From the results obtained from MMC piston, as in Tables 2.1 and 3.4, and Figures 4.20 and 4.21 respectively, it is clear that the stress induced in the MMC composite piston was found to be lower than that of the regular piston. Hence, replacement of piston material with the MMC will give increased strength, reduced weight, and reduced stress in the structure. A fuel saving of 0.34% was achieved, leading to lower running costs.

## **5.2 Recommendations**

The current study has provided some important information about the development and characterization of the microstructure and properties of Al-Si-Fe alloy, and its composite containing different weight fractions of CSA particles. In the course of the investigation, new areas of research have been identified.

- i. The age-hardening behaviour of the developed composite should be investigated.
- ii. It is recommended that further matrix-particle interface be investigated, using high-resolution transmission electron microscope
- iii. Finally, the National Automotive Council is persuaded to support further development of this novel material into commercial preposition.

## REFERENCES

- AbdulRahim, R. K. AbdulRazak and Mohammed S. A. D. (2014). Computational Fluid Dynamics (CFD) Analysis of Flow Field Development in a Direct Injection Diesel Engine with Different Manifolds, *American Journal of Fluid Dynamics*. 4(3), 102-113
- Aigbodion, V. S. and Hassan, S. B. (2010). Experimental Correlations between Wear Rate and Wear Particulate of Al-Cu-Mg/Bagasse Ash Particulate Composite. *Journal of Materials and Design*. 31(4), 2177-2180.
- Ajay, R. S., and Pushpendra, K. S. (2014). Design Analysis and Optimization of Three Aluminium Piston Alloys Using Finite Element Analysis, *International Journal of Engineering Research and Applications*, 4(13), 94-10
- American Society for Testing and Materials (ASTM) (2000) ASTM E 18-103-2000 and 790-99-2000. *American Standard of Testing and Materials (ASTM) Committee on Standards*.
- Anilkumar, H. C., Hebbar, H. S., and Ravishankar, K. S. (2011). Mechanical Properties of Fly Ash Reinforced Aluminium Alloy (Al 6061) Composite, *International Journal of Mechanical and Materials Engineering*, 1(6), 43-51
- Asif M., Chandra K., and Misra P. S. (2011). Development of Aluminium Based Hybrid Metal Matrix Composites for Heavy Duty Application. *Journal of Minerals and Materials Characterization and Engineering*. 10(14), 37-44
- Automotive Laboratory Kaduna Polytechnic (2019), , *Department of Mechanical Engineering*, Kaduna State, Nigeria
- Ayatollahi, M. R., Mohammadi, F., and Chamani, H. R. (2011). Thermo-Mechanical Fatigue Life Assessment of a Diesel Engine Piston, *International Journal of Automotive Engineering*, 1(4), 56-63
- Barekar, N., Tzamitzis, B., K., Dhindaw, J., Patel, N., and Haribabu, Z. (2008). Processing of Al-Graphite Particulate Metal Matrix Composites by Advanced Shear Technology. *Journal of Materials Engineering and performance*, 12(5), 52-61
- Bello, S.A., Hassan S.B., Agunsoye J.O., Zebase Kana M.G., and Raheem I.A. (2015). Synthesis of Un-carbonised Coconut Shell Nanoparticles: Characterisation and Particle Size Determination. *Tribology Industry*, 37(2), 257-263
- Bhagat, A. R., and Jibhakate, Y. M. (2011). Thermal Analysis and Optimization of I.C. Engine Piston Using Finite Element Method, *International Journal of Modern Engineering Research (IJMER)*, 2(4), 19-27,
- Bhattacharya, A. (2014). Analysis of piston of two stroke engine. *International Journal of research in engineering technology*, 3(6), 642-648
- Budynas, R. G., and Nisbett K. J. (2014). *Mechanical Engineering Design, a Text Book of Engineering Design*, New York, Mc Graw Hill Publishers
- Callister A. (2013). *Introduction to Material Science and Engineering*. New York, Jewel Publishers

- Chinthani, D. L., and Mevan P. (2015). A physic-Chemical analysis of coconut shell powder. *International Symposium on applied chemistry. Elsevier, Science Direct*, 16(2), 222-228
- Clyne, T. W (2013). Metal Matrix Composites. Matrix and Processing; Encyclopaedia of Materials Science and Technology: A Mortenson (Elsevier) (Pp. 1-20)
- Daljeet S., Harmanjit S. and Som K. (2012). An Experimental Investigation of Mechanical Behaviour of Aluminium by Adding Sic and Alumina. *International Journal on Emerging Technologies*, 6(2), 14-21
- Deborah D., L. (2019). Metal Matrix Composites. In Carbon Composites, Second Edition, Handbook of Non-Ferrous Metal Powder, Elsaviar Science Direct (Pp 390-407)
- DilipKumar, S. and Madhura, C. (2015). Theoretical Analysis of stress and Design of Piston Head using CATIA and ANSYS. *International Journal of Engineering Science Invention*, 4(6), 52-61
- Dinesh K., and Jasmet S., (2014). Investigation of mechanical properties of aluminium based hybrid metal composite. *International journal of engineering research application*. 8(3), 75–85.
- Enetaya, A. N. (2014).Improving natural organic fibre reinforced polymer composites for machine components. *Small and Medium Scale Conference, University of Benin Nigeria*, 2(9), 6-8.
- European Aluminium Association, (2015). *The Aluminium Automotive Manual, Application-Power Train Piston*: Rohrlé M. D.
- Fernando, L., and Hans, P. D (2010). Enhanced Young's Modulus of Al-Si Alloys and Reinforced Matrices by Co-continuous Structures, *Journal of Composites Materials*,5(24), 739-755
- Firdaus R. M., Supriyo B., and Suharjono A. (2020). Analysis of braking force efficiency measurements for various braking strategy applied for vehicle tested on roller brake tester. *Journal of Physics*, 3(22), 27-35
- Francis, U. (2012). Casting of motor cycle piston from aluminium piston scrap using metallic mould. *Leonardo Electronic Journal of practices and Technologies*, 4(21), 82-92
- Franz, X. T., and Seshasai S. (2009). Computational Fluid Dynamics (CFD) based optimization of fuel injection strategies in a diesel engine using an adaptive gradient method, *Applied Mathematica Model*, 33(3), 1366–1385
- Gaitondel, V. N., Karnik S.R and Javaprakash M.S (2012). Wear and Corrosion Properties of Al/Al<sub>2</sub>O<sub>3</sub>/Graphite Hybrid Composite. *Journal of Minerals and Materials Characterisation and Engineering*, 25(6), 695 - 705
- Hubert, C., Marteau, J., Deltombe, R., Chen, Y. M., and Bigerelle, M., (2014). Roughness Characterization of the Galling of Metals, Surface Topography, *Metrology and Properties*, 5(2), 1-9

- Ibrahim, N. M., Bakar, R. A., and Ismail, A. R. (2008). In-Cylinder Flow through Piston-Port Engines Modelling using Dynamic Mesh, *Journal of Applied Sciences Research*, 4(1): 58-64,
- Ismail, A. R., Soon, Y. C., Abdullah, B., Zulkifli, R., Sopian, K., and Rahman, M. N. (2009). Reverse Engineering in Fabrication of Piston Crown, *European Journal of Scientific Research*, 29(1), 136-146
- Issac, D., Ramasamy, S., and Nadajaram, S. (2016). Effect of Ceramic Particulate Type on Microstructure and Properties of Copper Matrix Composites Synthesis by Friction Stir Processing. Science Direct, *Journal of Materials Research and Technology*. 5(4), 302-316
- Itsko, G., Rohatgi, P. K., Moutsatsou, A., Rover H., J., Schultz, B., F., Koukouzas, N. and Vasilatos, C. (2011). Incorporation of High Ca Fly Ash Particles into A356Al by Stir Casting Technique and characterization of the Fabricated Composites. *World of Coal Ash (WOCA) Conference*. 35(8), 112-121
- Jadhav V., Jain R. K., and Yogendra S. C. (2016). Design and Analysis of Aluminium Alloy Piston using Computer Aided Engineering (CAE) Tools. *International Journal of Engineering Sciences and Research Technology*. 5(7), 332 - 339
- John, M. Fox, (2017). Fly Ash Classification, Old and New Ideas, *World of Coal Ash (WOCA) Conference in Lexington*, 23(4), 1-19
- Julian I. E. Hoffman, (2015). Biostatistics for Medical and Biomedical Practitioners. Science direct, *International Journal of applied science*. 4(3), 204-228
- Karthikaiselvi, R., and Subhashini, S. (2014). Study of the absorption properties and inhibition of mild steel corrosion in hydrochloric acid media by water soluble composite polyvinyl alcohol-omethoxy, *Journal of the Association of Arab Universities for Basic and Applied Sciences*, 16(2), 74-82
- Keneth, K., Moyosore, T., A., and Olubambi, A., P. (2014). Corrosion Behaviour of Al-Mg-Si Alloy Matrix Hybrid Composites Reinforced with Rice Husk Ash and Silicon Carbide. *Journal of Materials Research and Technology*, 3(1), 9-16
- Kenneth, K. A, Adetomolola, V. F, and Nthabiseng, B. M. (2018). Evaluation of damping behaviour of Al-Mg-Si alloy based composites reinforced with steel, steel and graphite, and silicon carbide particulate, *Engineering Science and Technology, International Journal of Materials Research and Technology, Elsevier*, 21(4), 798-805
- Kesavulu A., F. AnanRaju, M. L., and Devakumar S. (2014). Properties of Aluminium Fly Ash Metal Matrix Composite. *International journal of innovative research in science, engineering and technology* .3(11), 160- 171
- Kethavath, V., Dinesh, B., and Kumar, A. (2015). Design and Structural Analysis of Composite Piston. *International Journal & Magazine of Engineering, Technology, Management and Research*, 2(10), 464-470
- Khaleel, A., Ahad, A., and Hussain, M. (2016) Modelling and Optimization in a New Machining Production Line by Using Manufacturing System Simulation. *International Conference Proceedings on Industrial Engineering and Operations Management, Detroit, Michigan, USA*. 12(5), 869-879

- Khurmi, R.S, and Gupta, J.K. (2004). *A Text Book of Machine Design*, S. Chand & Co., New Delhi, India
- Kinshawy, H. A, (2019). Turning Processes for Metal Matrix Composites in Machining Technology for Composite Materials, *Handbook of Non-Ferrous Metal Powder*, 290-307, Elsevier Science Direct
- Kolbenschmidt Motor, (2017). Motor service (MS), *International, online catalogue*. Retrieved from [www.ms-motor-service.com/en/product-applications/catalogue](http://www.ms-motor-service.com/en/product-applications/catalogue)
- Larry S., (2016). Class C and Class F Fly Ash; Comparisons, Applications and Performance. Michigan Technology University. 16(4), 10-20
- Mahendra M., Boopathip P. A., and Iyan D. (2013). A Study on Evolution of Mechanical Properties of Fly Ash and Alumina Reinforced With Silicon Carbide and Fly Ash Composite. *American Journal of Applied Science*, 10(3), 219- 225
- Manish B. Shinde, Sakore T. V., and Katkan V. D. (2016). Design Analysis of Piston for Four Stroke Cylinder Engine using ANSYS. *International Journal of Current Engineering and Technology*, 6(4), 94 - 99
- Miltiadis A. B. (2010). CAD-CAM and Rapid Prototyping, Application and Evaluation, (1<sup>st</sup> ed.), *bookbon.com*, 53-61
- Monikandan, V. V, Joseph, M. A, and Rajendrakumar, P. K, (2016). Dry sliding wear of aluminium matrix hybrid composites, *Resource-Efficient Technologies, Elsevier*, 12(3), 12-24
- Nijssen, M. (2015). Composite materials an introduction to coir fibre *.Encyclopedia of science and technology. archive of mechanical engineering and material* 1(4), 73-78
- Ogbonnaya, E., A., Nwankojike, E., A., Adigio, E., A., Fadeyi, J., A., and Nwogu, C., N., (2013). Development of CNC Program for Piston Production, *International Journal of Engineering and applied Science*, 13(3), 32-39
- Oghenevweta, J. E, Aigbodion, V. S., Nyior, G. B., and Asuke, F. (2016). Mechanical properties and microstructural analysis of Al–Si–Mg/carbonized maize stalk waste particulate composites, *Journal of King Saudi University – Engineering Science*, 2(28), 222-229
- Oloruntoba, D. T., Popoola, A. P. I., and Falokun D. A. (2015). Investigation on water plant extract as a corrosion inhibitor for automobile engine and industry, *African Corrosion Journal*, 1(2), 9-15
- Orhorhoro, E. K., Oyiboruona, P. E., and Ikpe, A. E. (2017). Investigation and Evaluation of the Corrosion Inhibition Properties of Water Hyacinth Extract on Low Carbon Steel, *International Journal of Energy Engineering Research and Technology*, 5(12), 45-50
- Pardeep, S., Setpal, S., and Dinesh, K. (2016). Effect of Graphite Reinforcement on Physical and Mechanical Properties of Aluminium Metal Matrix Composites Particulate, *Science and Technology: An International Journal* 2 (34), 17-22

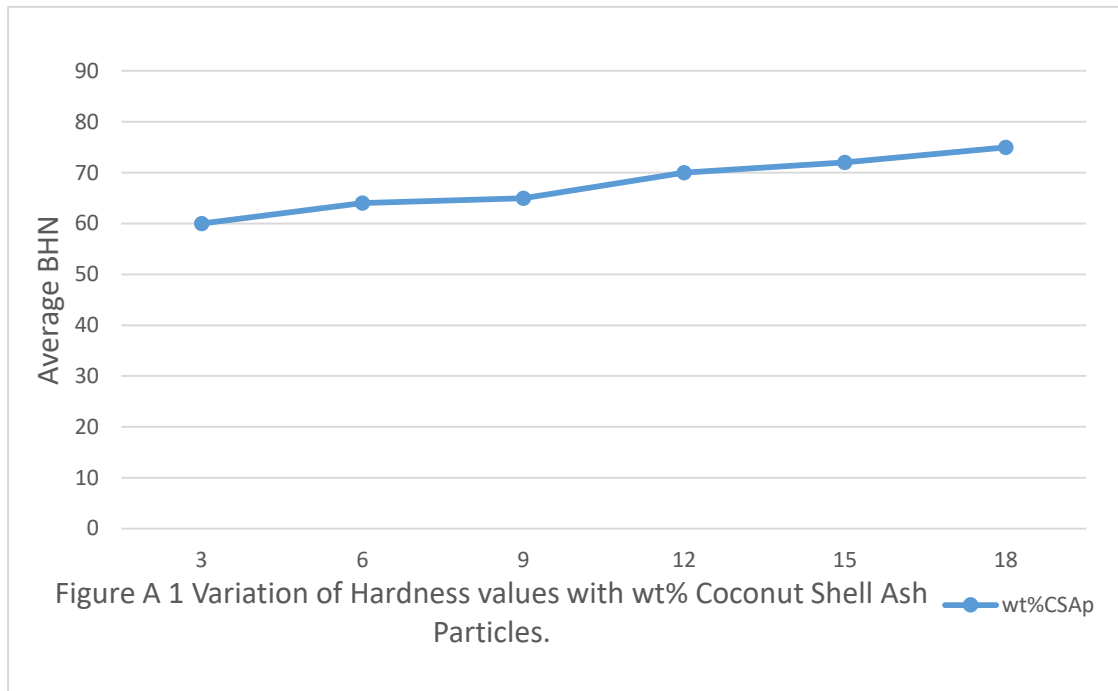
- Poornesh, M., Johnson, X. S., Jevy, S., and Gavin, M. P. (2017). Effect of Coconut Shell Ash and SiC Particles on Mechanical Properties of Aluminium Based Composites. *American Journal of Materials Science*, 7(4), 112-115
- Prasad G. S., dinesh K. A., Dileep Kumar K. G., Nagaraju M. and Srikanth K. (2016). Design and Analysis of Piston Internal Combustion Engine on Different Materials Using CAE Tools ANSYS. *International Journal of Innovative Research in Science, Engineering and technology*, 4(5), 6095-6103
- Prasad, D S., and Krishna, A.R (2010). Fabrication and Characterization of A356.2-Rice Husk Ash Composite using Stir Casting Technique. *International Journal of Science Engineering and Technology* 2(12), 7603-7608.
- Rao, D. M., and Raju, M. E, (2014). Preparation and Characterization of AL-Fly Ash Metal Matrix Composite by Stir Casting Method, *International Journal of Innovative Science and Modern Engineering (IJISME)*, 1(3), 1-5
- Razzak, A. M, Abdul Majid, D. L, Ishak, M. R., and Aday, M. B. (2017). Microstructural Characterization of fly ash Particulate Reinforced AA6063 Aluminium Alloy for Aerospace Application *IOP Conference Series: Material Science and Engineering*. 7(3), 1-6
- Rohatgi, P. K., Weiss, D., and Nikhil, G. (2006). Application of Fly Ash in Synthesizing Low- Cost MMCs for Automotive and other Applications, *International Journal of Science Engineering and Technology*, 3(58), 71-76
- Sandeep K. K., and Vishnu B. G. (2015). Design and Analysis of Piston by using Finite Element Analysis, *International Journal of Engineering Research and Technology*. 9(4), 296-301.
- Sharanabasappa, R. P., and Moti B. S. (2013). Study of Mechanical Properties of fly ash and Alumina Reinforced Aluminium Alloy. *Journal of Mechanical and Civil Engineering*. 2(7), 55 – 77.
- Shuogo, Z. (2012). Design the Piston of Internal Combustion Engine by Pro/ENGEER 2<sup>nd</sup> *International Conference on Electronic and Mechanical Engineering and Information Technology (EMEIT)*, 3(4), 26-33
- Silva, D., Sumit J., and Mayur, I. (2013). Design Analysis of a Circular and Square Shaped Piston Head Considering Mechanical Stresses Induced, *International Journal of Mechanical Engineering Research & Applications (IJMERA)*, 5(1), 23-31
- Sivaramakrishnan K., Jithendra G, and Ajith V. K., (2019) Design and Analysis of Four Stroke Engine Piston, *International Journal of Engineering Science and Computing*, 9(2), 743-746
- Sushma, H., and Jagadeesha, K. B. (2013). Computational Fluid Dynamics (CFD) Modelling of the In-Cylinder Flow in Direct Injection Diesel Engine. *International Journal of Scientific and Research Publication* 3(2), 22-31
- Tadala A.,Naresh K., Abdul K., and Purushotham A. K., (2016) Analysis on Four Stroke Single Cylinder Engine Piston by using Aluminium Alloys (Al-GHS 1300, Al-Sic-Graphite, A6061Pure Aluminium) *International Journal of Mechanical Engineering*, 1(3), 4-11

- Udhayasankar, R., and Karthikeyan, B. (2015). A review on Coconut Shell Reinforced Composites. *International Journal of Chem Tech Research*. 11(8), 624-637
- Veereshkumar, G. B., Rao, C. S., Salvaraj, N., and Bhagyashekar, M. S. (2011). Studies on Al6061-SiC and Al7075-Al<sub>2</sub>O<sub>3</sub> Metal Matrix Composites. *Journal of Minerals and Materials Characterization and Engineering*. 9(1), 43-55
- Venkata, C. R., Murthy P.V, Murali M.V., and Rao G.M (2013). Design Analysis and Optimization of Piston using CATIA and ANSYS, *International Journal of Innovative Research in Engineering & Science*, 2(1), 41-51
- Venkatesh, K., and Viveknanda, S (2014) Structural Analysis and Manufacturing Process Optimization of an Aerospace Component. *International Journal of Mechanical Engineering and Robotic Research*, 2(4), 632-641
- Venkateswara, K., and Baswaraj, H. (2014). Modelling analysis and Optimization of Diesel Engine Piston. *International Journal of Research and Engineering and Advanced Technology (IJREAT)*, 2(1), 21-29
- Verma V. and Khvan A. (2019). A Short Review on Al MMC with Reinforcement Addition Effect on their Mechanical and Wear Behaviour, *Advances in Composite*, Retrieved from <https://www.intechopen.com/books/advances-in-composite-materials-doi:10.5772/intechopen.83584>
- Vinod Y., and Mittal N., D. (2013) Design and Analysis of Piston Design for 4 Stroke Hero Bike Engine, *International Journal of Engineering Innovation & Research*, 2(2), 148-150
- Vorozhtsov, S., Zhukov, I., Vorozhtsov, A., Zhukov, A., Eskin, D., and Kvetinskaya, A. (2015). Synthesis of Micro- and Nanoparticles of Metal Oxides and Their Application for Reinforcement of Al-Based Alloys, *Advances in Materials Science and Engineering*, 2(4), 6-11
- World of Coal Ash Conference (WOCA) (2017), An international conference organized by the American Coal Ash Association (ACAA) and the University of Kentucky Center for Applied Energy Research (CAER). Lexington, Kentucky USA <http://www.worldofcoalash.org/index.html>
- Yuan, G., Jin-Chuan J., Peng-Chao Z., Jian Z., Tong, W., and Ting-Ju, L. (2015). Wear behaviour of High Strength and High Conductivity Cu-Alloy under dry sliding. *Science Direct, Elsevier*, 25(7), 2293-2300

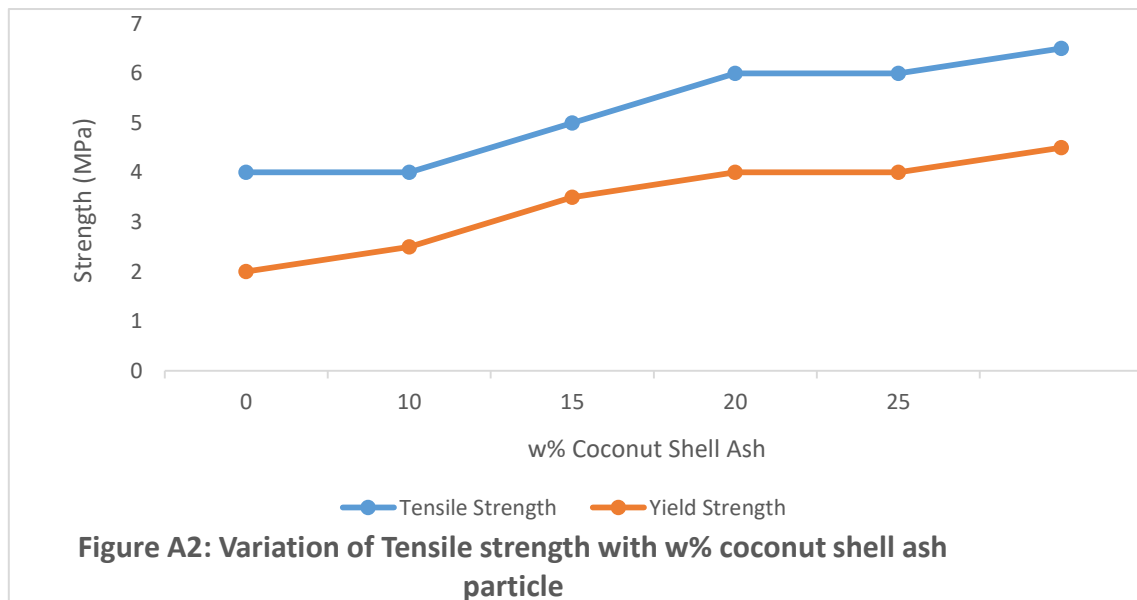


## APPENDICES

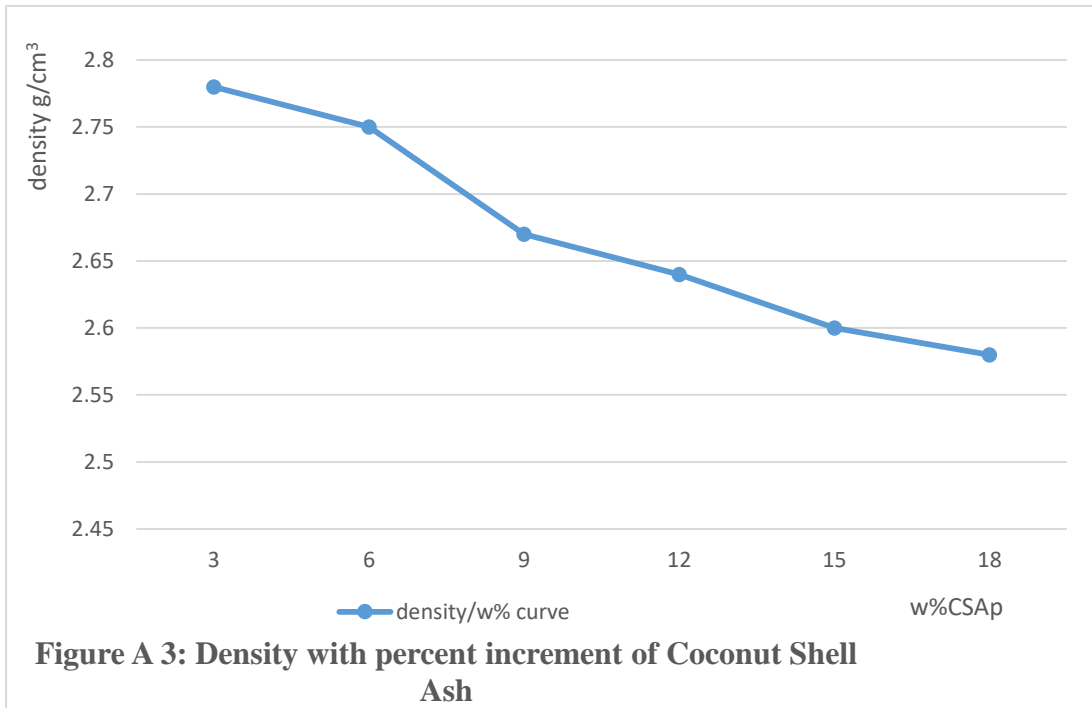
### APPENDIX A1: Plots of Hardness Test



### APPENDIX A2: Plot of Tensile Strength and Yield Strength



### APPENDIX A3: Plot of Density of with Increasing Coconut Shell Ash Wt%



### APPENDIX A4: Plot of Wear Rate

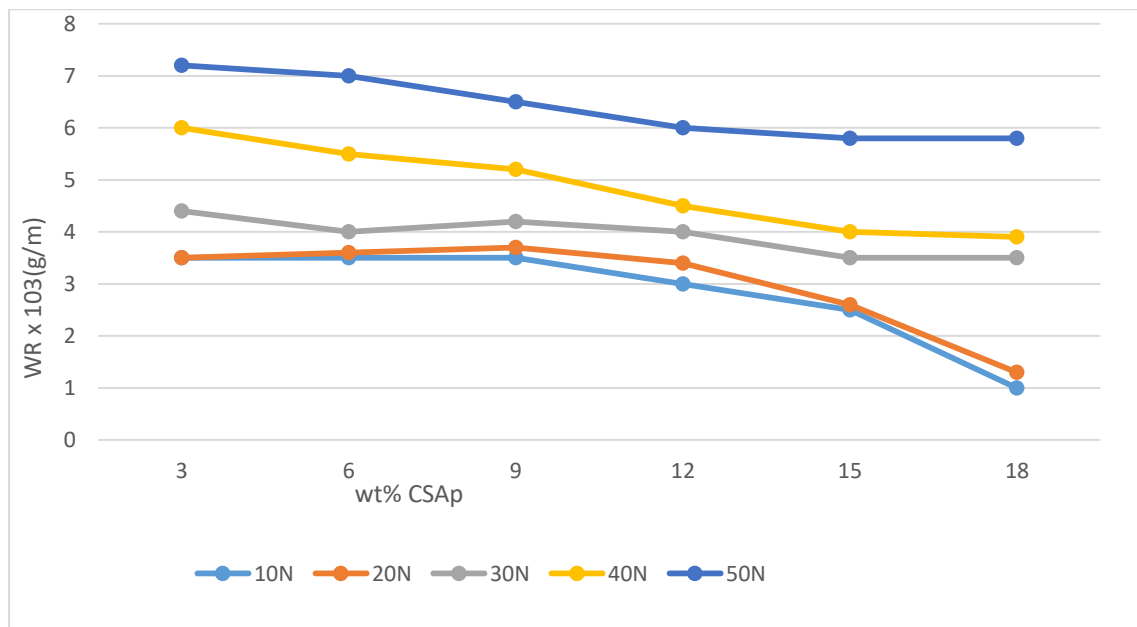


**Figure A 4: Variation of wear rate with wt% of coconut shell ash particles**

**APPENDIX A5: Plot of Coefficient of Friction**

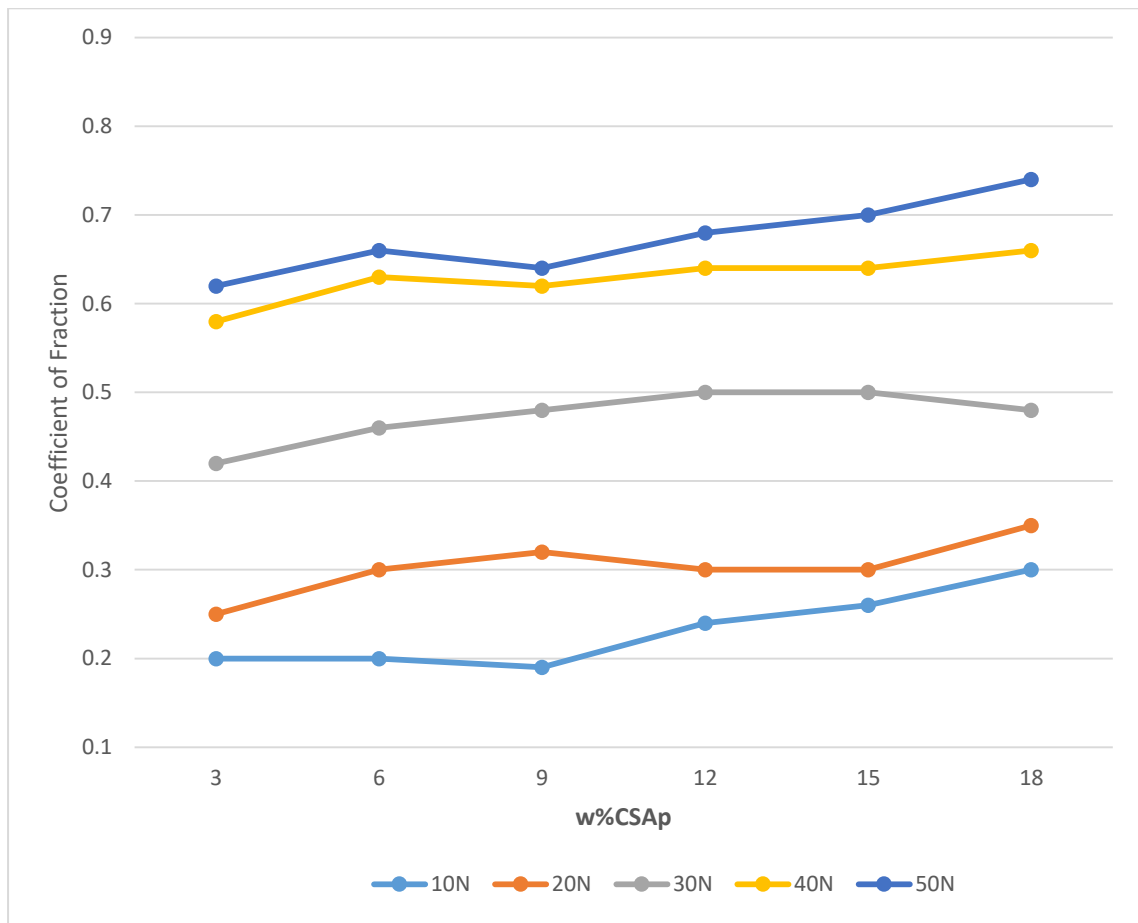


**Figure. A5: Variation of Coefficient of Friction with w% of Coconut Shell Ash**

**APPENDIX A6: Plot of Corrosion Rate**

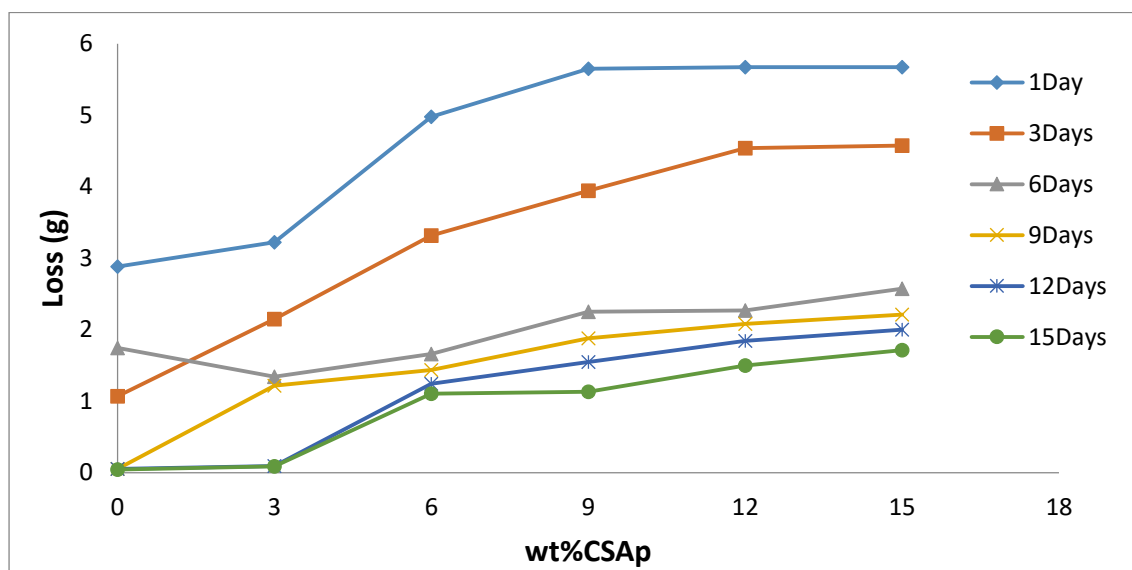


**Figure: A6: Average Corrosion Rate Al-Si-Fe/Coconut Shell Ash (CSAp) Composites Immersed In 3.5%NaCl Solution**

## APPENDIX B

### APPENDIX B1: Fuel Consumption per KWh for Conventional Standard Piston

For 0.1 litres of fuel,  $\frac{0.1 \times 60 \times 60}{16.5 \times 60} = 0.36$

For 0.2 litres of fuel,  $\frac{0.2 \times 60 \times 60}{20 \times 60} = 0.60$

For 0.3 litres of fuel,  $\frac{0.3 \times 60 \times 60}{24 \times 60} = 0.75$

For 0.4 litres of fuel,  $\frac{0.4 \times 60 \times 60}{30 \times 60} = 0.80$

### APPENDIX B2: Fuel Consumption per KWh of the Produced Composite Piston

For 0.1 litres of fuel,  $\frac{0.1 \times 60 \times 60}{18 \times 60} = 0.33$

For 0.2 litres of fuel,  $\frac{0.2 \times 60 \times 60}{22 \times 60} = 0.55$

For 0.3 litres of fuel,  $\frac{0.3 \times 60 \times 60}{28 \times 60} = 0.64$

For 0.4 litres of fuel,  $\frac{0.4 \times 60 \times 60}{33 \times 60} = 0.73$